TKK Dissertations 204
Espoo 2009

# CHARACTERIZATION AND ANALYSIS OF PHOTODARKENING IN DOUBLE CLADDING YTTERBIUM-DOPED SILICA FIBERS

Doctoral Dissertation

**Mikko Söderlund**

**Helsinki University of Technology**
**Faculty of Electronics, Communications and Automation**
**Department of Micro and Nanosciences**

TKK Dissertations 204
Espoo 2009

# CHARACTERIZATION AND ANALYSIS OF PHOTODARKENING IN DOUBLE CLADDING YTTERBIUM-DOPED SILICA FIBERS

Doctoral Dissertation

**Mikko Söderlund**

Dissertation for the degree of Doctor of Science in Technology to be presented with due permission of the Faculty of Electronics, Communications and Automation for public examination and debate in Large Seminar Hall of Micronova at Helsinki University of Technology (Espoo, Finland) on the 4th of December, 2009, at 12 noon.

**Helsinki University of Technology**
**Faculty of Electronics, Communications and Automation**
**Department of Micro and Nanosciences**

**Teknillinen korkeakoulu**
**Elektroniikan, tietoliikenteen ja automaation tiedekunta**
**Mikro- ja nanotekniikan laitos**

Distribution:
Helsinki University of Technology
Faculty of Electronics, Communications and Automation
Department of Micro and Nanosciences
P.O. Box 3500 (Tietotie 3)
FI - 02015 TKK
FINLAND
URL: http://nano.tkk.fi/
Tel. +358-9-470 23121
Fax +358-9-470 25008
E-mail: mikko.soderlund@tkk.fi



ISBN 978-952-248-247-1
ISBN 978-952-248-248-8 (PDF)
ISSN 1795-2239
ISSN 1795-4584 (PDF)
URL: http://lib.tkk.fi/Diss/2009/isbn9789522482488/

TKK-DISS-2688

Multiprint Oy
Espoo 2009

| ABSTRACT OF DOCTORAL DISSERTATION | HELSINKI UNIVERSITY OF TECHNOLOGY<br>P. O. BOX 1000, FI-02015 TKK<br>http://www.tkk.fi |
|---|---|

Author Mikko Söderlund

Name of the dissertation

Characterization and analysis of photodarkening in double cladding ytterbium-doped silica fibers



| Manuscript submitted 25.9.2009 | Manuscript revised 13.11.2009 |
|---|---|
| Date of the defence 4.12.2009 | |
| ☐ Monograph | ☒ Article dissertation (summary + original articles) |

| | |
|---|---|
| Faculty | Faculty of Electronics, Communications and Automation |
| Department | Department of Micro and Nanosciences |
| Field of research | Photonics |
| Opponent(s) | Dr. Jose Salcedo |
| Supervisor | Prof. Seppo Honkanen |
| Instructor | |




Abstract

Ytterbium-doped double cladding fibers have emerged as an excellent solution for power scaling of diffraction-limited high peak and average power laser sources. However, the photodarkening effect, which manifests as progressive growth of loss leading to degradation of laser performance, poses a very serious threat to the reliability of ytterbium-doped fiber lasers.

This thesis is focused on developing methods to quantify the photodarkening process and associated thermal processes in ytterbium-doped aluminosilicate fibers. Inversion was found to be a key controlling variable in the forward photodarkening process. However, three thermal processes were observed that affect the photodarkening kinetics and therefore complicate the interpretation of kinetic data. A photodarkened sample was measured to exhibit further heat-induced darkening when subjected to elevated temperatures. In addition, photodarkening-induced absorption spectrum was found to exhibit heat-induced spectral broadening with the loss-change having a linear dependence on temperature proportional to $|\lambda-\lambda_0|$. For the studied fiber, $\lambda_0$ was found to be 612 nm. Thermal activation energy distribution of the photodarkening-induced defects was measured to be governed by a single defect with the peak located at 1.32 eV with a FWHM of 0.31 eV. Furthermore, temperature of the fiber was found to correlate with the pump power absorbed by the photodarkening-induced defects. The observed thermal processes are therefore progressively being activated during pumping, unless isothermal conditions are being maintained. Finally, a manifestation of the photodarkening rate dependence on inversion, i.e., transverse photodarkening-induced loss variation, was observed by comparing the near-field intensity distributions of a pristine and a photodarkened fiber.

In addition to work related to photodarkening, this dissertation includes a theoretical study on the inversion, gain, and amplified spontaneous emission behaviour in a cladding-pumped erbium-doped fiber. Increasing the cladding area was found to result in a more uniform inversion distribution along the fiber length, therefore preventing short-wavelength gain and ASE build-up and improving the quantum conversion efficiency.




| Keywords | ytterbium, photodarkening, optical fiber, color center | |
|---|---|---|
| ISBN (printed) | 978-952-248-247-1 | ISSN (printed) 1795-2239 |
| ISBN (pdf) | 978-952-248-248-8 | ISSN (pdf) 1795-4584 |
| Language | English | Number of pages 62 + approx. 43 |
| Publisher | Helsinki University of Technology, Department of Micro and Nanosciences | |
| Print distribution | Helsinki University of Technology, Department of Micro and Nanosciences | |

☒ The dissertation can be read at http://lib.tkk.fi/Diss/2009/isbn9789522482488/

| VÄITÖSKIRJAN TIIVISTELMÄ | TEKNILLINEN KORKEAKOULU<br>PL 1000, 02015 TKK<br>http://www.tkk.fi |
|---|---|

Tekijä Mikko Söderlund

Väitöskirjan nimi

Valon aiheuttaman vaimennuksen karakterisointi ja analysointi ytterbium-seosteisissa kaksoiskuorikuiduissa

| Käsikirjoituksen päivämäärä 25.9.2009 | Korjatun käsikirjoituksen päivämäärä 13.11.2009 |
|---|---|
| Väitöstilaisuuden ajankohta 4.12.2009 | |
| ☐ Monografia | ☒ Yhdistelmäväitöskirja (yhteenveto + erillisartikkelit) |

| | |
|---|---|
| Tiedekunta | Elektroniikan, tietoliikenteen ja automaation tiedekunta |
| Laitos | Mikro- ja nanotekniikan laitos |
| Tutkimusala | Fotoniikka |
| Vastaväittäjä(t) | Dr. Jose Salcedo |
| Työn valvoja | Prof. Seppo Honkanen |
| Työn ohjaaja | |


Tiivistelmä

Ytterbium-seosteinen kaksoiskuorikuitu on osoittautunut erinomaiseksi rakenteeksi diffraktiorajoitteisten pulssitettujen ja jatkuvatehoisten laserlähteiden ulostulotehon skaalaamisessa. Ytterbium-seosteisten kuitulasereiden luotettavuuden uhaksi on kuitenkin muodostunut valon aiheuttama vaimeneminen, niin sanottu photodarkening-ilmiö, joka ajan myötä heikentää laserin hyötysuhdetta ja ulostulotehoa.

Tässä työssä on tutkittu erityisesti photodarkening-ilmiötä ja kehitetty menetelmiä sen etenemisen sekä siihen liittyvien termisten prosessien määrittämiseksi. Inversion havaittiin olevan määräävässä asemassa photodarkening-ilmiön etenemisessä. Toisaalta työssä havaittiin kolme termistä prosessia, jotka vaikuttavat häviön suuruuteen, ja siten muun muassa vaikeuttavat tarkan inversio-riippuvuuden määrittämistä. Valon aiheuttaman vaimennuksen havaittiin kasvavan säteilytyksen jälkeen kuidun lämpötilaa kasvattaessa. Tämän lisäksi aiheutuneen vaimennusspektrin havaittiin olevan riippuvainen kuidun lämpötilasta siten, että vaimennuksen muutos on suhteessa aallonpituuseroon $|\lambda\text{-}\lambda_0|$, jossa $\lambda_0$ on 612 nm mitatulle kuidulle. Photodarkening-prosessissa syntyneiden lasin virheiden aktivointienergiajakauman määritettiin keskittyvän 1.3 eV:iin sen puoliarvoleveyden ollessa 0.31 eV. Mitattavan kuitunäytteen lämpötilan havaittiin korreloivan vaimennukseen absorboituneen pumpputehon kanssa. Näin ollen havaitut termiset prosessit ovat aktiivisia ja voimistuvat mittauksen aikana, ellei näytteen lämpötilaa kontrolloida. Tämän lisäksi mitattauksella osoitettiin todeksi inversion paikallisesta vaihtelusta aiheutuva poikittainen vaimennusjakauma kuidun ytimessä.

Photodarkening-ilmiön tutkimuksen lisäksi tässä työssä mallitettiin inversion, vahvistuksen ja vahvistuneen spontaanin emission käyttäytymistä kuoripumpatussa erbium-seosteisessa kuidussa. Kuorikerroksen pinta-alan kasvattamisen havaittiin johtavan tasaisempaan pitkittäiseen inversiojakaumaan, jonka johdosta lyhyen aallonpituuden vahvistus ja kohina pieneni ja vahvistimen kvanttihyötysuhde parani.



| | | | |
|---|---|---|---|
| Asiasanat | ytterbium, photodarkening, optinen kuitu, värikeskus | | |
| ISBN (painettu) | 978-952-248-247-1 | ISSN (painettu) | 1795-2239 |
| ISBN (pdf) | 978-952-248-248-8 | ISSN (pdf) | 1795-4584 |
| Kieli | Englanti | Sivumäärä | 62 + n. 43 |
| Julkaisija | Teknillinen Korkeakoulu, Mikro- ja nanotekniikan laitos | | |
| Painetun väitöskirjan jakelu | Teknillinen Korkeakoulu, Mikro- ja nanotekniikan laitos | | |

☒ Luettavissa verkossa osoitteessa http://lib.tkk.fi/Diss/2009/isbn9789522482488/

# Preface

This dissertation is a summary of research work carried out mainly at Helsinki University of Technology (HUT), Photonics group, between 2007-2009. However, the basis for this work was built in the Product Development team at Liekki Oy during 2004-2007, and even earlier at the Photonics group at Technical Research Center of Finland (VTT) between 1999-2004. I am very furtunate to have had the opportunity to work in great teams and with great (if not the best) people. Especially, I have been priviliged to work with the following individuals/teams: Prof. Seppo Honkanen, who in 2007, welcomed me to his newly formed group and who's support, commitment, enthusiasm, and friendship I value greatly, Dr. Simo Tammela, who has mentored me in photonics research since 1996 and from whom I'v learned so much about the curious mind, Dr. Joona Koponen and Joan Montiel i Ponsoda, with whom I hade had the best, the deepest and the (photo)darkest discussions/collaboration on the dissertation topic, Dr. Jeffrey Koplov and Dr. Dahv Kliner, to whom I am greatfull for their experimental ideas and inspiration, many moments of laughter, and "knit picking" when I needed it (= Jeff had an instrumental role in correcting the text and figures in Publ. IV-V), co-workers at Liekki, who's persistance I admire and with whom I had some of the most unforgettable professional experiences, co-workers at TKK, especially Ari Tervonen for invaluable discussions, and Antti Säynätjoki, who tutored me with LaTeX, and co-workers at VTT and Prof. Matti Leppihalme, who supported me in the beginning of this journey.

I would also like to thank my mother Ritva for all her support and care, both for me and my family. Finally, thank you Tuulikki for your love and patience during all these years. And my children Aava and Julia - I love you, you are so precious!

Mikko Söderlund Helsinki, November 2009

# Contents

# List of Publications

This dissertation consists of an overview and of the following Publications which are referred to in the text by their Roman numerals.

**I** M. Söderlund, S. Tammela, P. Pöyhönen, M. Leppihalme, and N. Peyghambarian, "Amplified spontaneous emission in cladding-pumped L-band erbium-doped fiber amplifiers," IEEE Photon. Technol. Lett. **13**, 22-24 (2001)

**II** J. J. Koponen, M. J. Söderlund, H. J. Hoffmann, and S. K. T. Tammela, "Measuring photodarkening from single-mode ytterbium doped silica fibers," Opt. Express **14**, 11539-11544 (2006)

**III** J. Koponen, M. Söderlund, H. J. Hoffman, D. A. V. Kliner, J. P. Koplow, M. Hotoleanu, "Photodarkening rate in Yb-doped silica fibers," Appl. Opt. **47**, 1247-1256 (2008)

**IV** M. J. Söderlund, J. J. Montiel i Ponsoda, J. P. Koplow, and S. Honkanen, "Heat-induced darkening and spectral broadening in photodarkened ytterbium-doped fiber under thermal cycling," Opt. Express **17**, 9940-9946 (2009)

**V** M. J. Söderlund, J. J. Montiel i Ponsoda, J. P. Koplow, and S. Honkanen, "Thermal bleaching of photodarkening-induced loss in ytterbium-doped fibers," Opt. Lett. **34**, 2637-2639 (2009)

**VI** M. J. Söderlund, J. J. Montiel i Ponsoda, S. K. T. Tammela, K. Ylä-Jarkko, A. Salokatve, and S. Honkanen, "Mode-induced transverse photodarkening loss variations in large-mode-area ytterbium doped silica fibers," Opt. Express **16**, 10633-10640 (2008)

# Author's contribution

For Publication I, the author developed the simulation tool, participated in planning the simulations, conducted all the simulations, did the data analysis and prepared the manuscript.

For Publication II, the author lead the design of the experiment and conducted the preliminary measurements. The author also participated in the data analysis and preparation of the manuscript.

For Publication III, the author participated in the design of the experiments and preparation of the manuscript.

For Publication IV, the author participated in the design of the experiments, had a major role in conducting the experiments and in the data analysis and prepared the manuscript.

For Publication V, the author designed the experiments, had a major role in conducting the experiments, did the data analysis and prepared the manuscript.

For Publication VI, the author designed the experiments, conducted the experiments, did the data analysis and prepared the manuscript.

# List of Abbreviations

ASE amplified spontaneous emission

CW continuous wave

DCF double cladding fiber

DND direct nanoparticle deposition

EDFA erbium-doped fiber amplifier

ESA excited state absorption

HOM higher order mode

LMA large-mode-area

MFD mode field diameter

MCVD modified chemical vapor deposition

NA numerical aperture

NIR near-infrared

PCE power conversion efficiency

QCE quantum conversion efficiency

RE rare earth

RIP refractive index profile

SBS stimulated Brillouing scattering

SMF singlemode fiber

SRS stimulated Raman scattering

UV ultra-violet

# 1 Introduction

Fiber lasers offer many advantages over conventional solid-state lasers due to their diffraction-limited beam quality, high efficiency, good thermal management, mechanical robustness and versatility. Fiber lasers may be used as continuous wave (CW) sources in the kW output power regime [1], to amplify nanosecond pulses to MW peak powers [2] and to produce ultra-short pulses in the picosecond regime [3]. Through frequency doubling and tripling, wavelengths in the green to ultra-violet (UV) regions can be accessed [4]. Owing to this versatility, fiber lasers are used today in a broad range of applications ranging from industrial machining to medical applications.

The rapid development of fiber lasers since the year 2000, as seen by the tremendous increase of the average output powers of ytterbium-doped fiber lasers operating at 1.0 $\mu$m, can largely be attributed to the invention of the double cladding fiber structure [5], the subsequent development of large-mode-area (LMA) ytterbium-doped fibers, and methods to maintain single-transverse-mode propagation [6]-[8]. Furthermore, significant advances have been made in increasing the brightness and reliability of multimode pump diode sources and in the development of robust pump-coupling approaches, making kW range pump powers accessible. The 1.5 $\mu$m fiber laser sources based on erbium- and erbium/ytterbium-doped fibers are less efficient than their Yb-doped counterparts and therefore face challenges with thermal management. However, there is also a growing interest in power scaling fiber lasers whose operating wavelength permits the use of several orders of magnitude higher eye-safe exposure levels what the 1.0 $\mu$m emission from the Yb-doped fiber lasers allows.

In light of the progress made in power scaling of Yb-doped fiber lasers, it is surprising that research and systematic study of the photodarkening effect in Yb-doped fibers

took off as late as 2005, when the first scientific papers, i.e., Publication II and a preceeding conference paper [9], were published about it. Since then, photodarkening has been widely recognized as a threat to the reliability of Yb-doped fiber laser sources. This threat is largely associated with reduced efficiency and output power due to photodarkening-induced spectrally broadband loss which overlaps with the operating wavelengths at 1.0 $\mu$m. Today, several groups are actively studying this effect, and progress has been made in, for example, mitigation of the induced loss through compositional optimization.

The aim of this dissertation is to characterize the photodarkening effect and to develop accurate and repeatable measurement methods which contribute to an improved understanding of the underlying photo-chemical mechanism. Special focus is given to the thermodynamic properties of the photodarkening-induced defects. In addition, a simulation study on propagation of amplified spontaneous emission in a cladding-pumped erbium-doped fiber amplifier (EDFA) is conducted.

This dissertation is organized into seven sections. Chapter 2 gives an overview of power scaling methods and fundamental limitations of diffraction-limited fiber sources. Chapter 3 describes a numerical double cladding fiber model and presents simulation results for a cladding-pumped EDFA and for a short Yb-doped sample used in the photodarkening measurements. Chapter 4 is a review of the photodarkening effect in Yb-doped fibers, while chapter 5 focuses on the more recent work on thermodynamic analysis of photodarkening. Chapter 6 is devoted to the study of a specific manifestation of photodarkening, i.e., transverse photodarkening loss variations. In chapter 7, implications of the derived thermodynamic properties of photodarkening-induced defects are discussed. And to conclude, a summary and future prospects are found in chapter 8. In this dissertation, emphasis is put into providing a broader perspective on the research than what was possible in the individual Publications I-VI.

# 2 Power-scaling of rare-earth doped fiber lasers

In this dissertation, the term "power scaling" is used to refer to efforts in increasing the output power of diffraction-limited (i.e. single-transverse-mode) silica fiber based sources with step-function core refractive index profiles (RIP). When doped with some rare earth ion for producing gain, the conventional singlemode fiber (SMF) geometry (with roughly a 9-$\mu$m core diameter), is limited in achievable output power and extractable energy largely due to the growth of amplified spontaneous emission (ASE) [10]. Also, the thresholds of non-linear effects, such as Raman- and Brillouin-scattering, occur at relatively modest output powers in an SMF due to a small core area and a subsequent high signal intensity. Another limitation is imposed by the available pump power, which in a conventional amplifier configuration is limited to the use of several low-power single-mode pump sources. To scale such a configuration in power, one would have to apply hundreds of such sources to reach >10 W power regime and face problems with heat management and the high cost-structure of such a configuration. Considering all these limitations, a standard singlemode fiber geometry does not allow significant scaling of the output power. The aim of this chapter is to give an overview of the practical methods for power scaling of diffraction limited fiber sources, to describe the fundamental limitations, and to discuss the trade-offs involved regarding designs.

## 2.1 Double cladding fiber

A major breakthrough in the development of high-power fiber sources was the invention of a double cladding fiber (DCF) structure [5], schematics of which is presented in Fig. 2.1(a). In a DCF, the fiber core with a refractive index $n_1$ is surrounded by a lower refractive index ($n_2$) cladding layer, with the resulting core numerical

aperture ($NA_{core}$) given by

$$NA_{core} = \sqrt{n_1^2 - n_2^2}. \tag{2.1}$$

The pump light is coupled into and propagates in the cladding layer, guided by the refractive index difference between the glass cladding and the surrounding lower index layer ($n_3$), typically consisting of a fluoroacrylate polymer providing $NA_{clad} \leq 0.45$ for the pump waveguide. Alternatively, a fluorine doped silica glass layer is used with typically $NA_{clad} \leq 0.22$. The latter structure is referred to as an all-glass fiber, although the secondary glass cladding is usually also coated with a polymer for mechanical durability. To promote efficient pump absorption in the pump cladding, i.e., to minimize skew rays having low overlap with the doped core, shaping of the pump cladding, such as the octagonal shape illustrated in 2.1(a), is used [11].

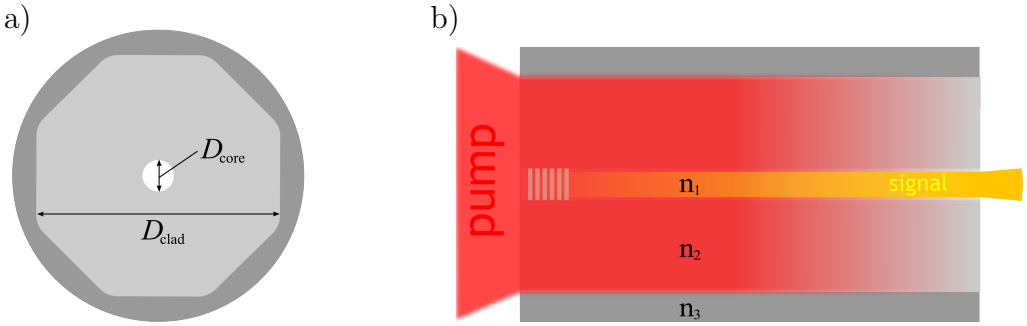


**Figure 2.1**: (a) A cross-section of a double cladding fiber structure and (b) its side-image illustrating the operating principle.

The small signal absorption coefficient $\alpha_p$(in units of dB/m) of the pump in a DCF is to the first order approximately given by

$$\alpha_p = \alpha \frac{A_{core}}{A_{clad}} = \alpha \left( \frac{D_{core}}{D_{clad}} \right)^2, \tag{2.2}$$

where $\alpha$ is the core material absorption coefficient and $A$ and $D$ stand for the area and diameter of the core or the cladding region, respectively. This approximation is reasonably accurate for DCFs with a shaped (e.g. octagonal) pump cladding. For

circular pump claddings, and for long lengths of fiber with a shaped cladding, the pump absorption coefficient can significantly deviate from the above approximation [12]. For the efficient use of the pump light, it is typically desirable to have a total small signal pump absorption $\alpha_p L \geq 20$ dB (i.e. $\geq$99 % absorption). A large pump cladding area facilitates the use of high-power, low brightness diode sources, thus reducing the number of individual pumps (i.e. cost), and complexity of the pumping configuration. Such sources are today commercially available in the wavelength range 800-976 nm either as single-emitter diode lasers in the 1-10 W power level or configured as bars with output power in the 10-100 W range. Compared to bulk solid-state lasers and core-pumped fibers, the DCF structure facilitates heat removal by spreading the heat load over a longer distance (i.e. larger surface area).

There are several ways to launch the pump power into the DCF. In end pumping, depicted in Fig. 2.1(b), the pump power (shown in red) is imaged onto the DCF pump waveguide so that both the pump beam diameter and launch $NA$ are within the acceptance values of the DCF. In a more robust and practical design, several fiber coupled diodes are combined into the DCF through a fused fiber coupled component [13]. Pumping methods relying on the principle of coupling the pump light from the side of the active fiber are also used, with the added advantage of giving an easy access to the core of the active fiber [14]-[16], an important consideration for high-power master-oscillator power-amplifier (MOPA) configurations . Figure 2.1(b) also illustrates the DCFs role as a "brightness enhancer". The pump power propagating in the cladding is absorbed in the RE-ion doped core and converted to a beam of different wavelength and of lower power, but with a diffraction limited beam quality. The narrowly spaced grid in the core of the fiber at the pump input end of the DCF illustrates another crucial fiber laser component: the fiber Bragg grating (FBG). In short, it is used to form a laser cavity and to direct the power in a controllable way out from one end of the cavity as a beam with narrow wavelength band.

## 2.2 Rare-earth dopants

The first fiber laser demonstration with a DCF structure used neodymium (Nd) as the gain medium [5]. Neodymium is usually pumped at 805 nm, and has its strongest emission peak at 1.06 $\mu$m. Lasing can also be achieved between 900-950 nm, but at an efficiency much reduced from that of the 1064 nm transition. An important performance figure of a laser system is the quantum defect, defined as the difference between the pump and signal photon energies, i.e.

$$q = h\nu_p - h\nu_s = h\nu_p \left(1 - \frac{\lambda_p}{\lambda_s}\right), \tag{2.3}$$

where $h$=6.626·10$^{-34}$ Js is the Planck constant, and $\nu_{p,s}$ is the pump or signal frequency. Quantum defect gives the minimum fraction (as given by the term in paranthesis) of absorbed pump that is dissipated as heat. For Nd transition at 1.06 $\mu$m $q$ is ∼24 %, and therefore significant fraction of the absorbed pump energy is lost as heat. For this reason, and due to higher emission bandwidth and longer excited state lifetime of the Yb-ion, Nd-fibers have been largely replaced by Yb-fibers in the 1.0 $\mu$m gain regime. However, when operated in the 1064 nm transition, Nd-ion is a true four level energy system, i.e., there is no ground state absorption (GSA). A Nd-doped fiber therefore has a much lower lasing threshold than an Yb-doped fiber, which may raise interest in the use of Nd-doping in some high efficiency, medium power fiber laser applications.

Erbium is the most important of the rare-earth ions due to the invention of the erbium-doped fiber amplifier in 1985 and its widespread use in the field of optical communication technology [17],[18]. The operating principle of erbium ions in producing amplification is illustrated in the simplified energy level diagram in Fig. 2.2(a). Pump excitation can take place at 980 nm or 1480 nm. Excitation to the $^4I_{11/2}$ state (i.e. 980 nm pump) leads to a fast non-radiative decay to the metastable $^4I_{13/2}$ state that has a long excited state lifetime (∼10 ms). Resonant pumping at 1480 nm corresponds to the transition between the lowest sub-level of the $^4I_{15/2}$ state

manifold to the highest lying sub-level of the $^4I_{13/2}$ state manifold. This splitting of the energy levels indicated in 2.2(a) is due to the electric field induced by the host glass, i.e. the Stark effect [19]. Rapid thermalization within the energy state manifold leads to a largely homogenous broadening of the transition lines, as illustrated by the smooth absorption and emission cross-sections measured for an aluminosilicate erbium-doped fiber in Fig. 2.2(b). Amplification takes place between the two state manifolds through the process of stimulated emission.

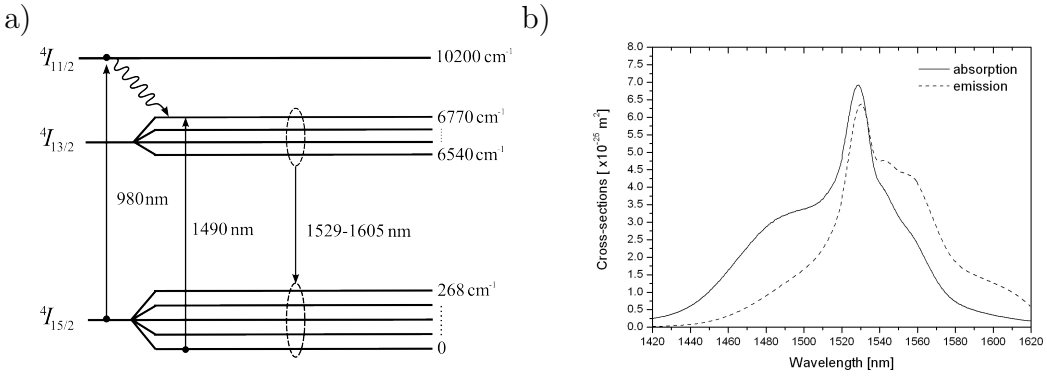


**Figure 2.2**: (a) Energy level diagram of erbium illustrating ground and excited state manifolds and transitions between the levels and sub-levels and (b) absorption and emission cross-sections of erbium in aluminosilicate glass.

An erbium-doped fiber pumped at 980 nm has a quantum defect of ∼37 %, and therefore is not the optimal choice from the power scaling point of view. Another limitation of erbium ion is the relatively low achievable doping concentration level before various ion-to-ion interactions begin to degrade the efficiency. Co-doping erbium with ytterbium has been used to circumvent the relative low pump absorption in erbium-doped fibers [20]. Pump energy absorbed by the Yb-ion is transferred to the neighbouring Er-ion, promoting it to the $^4I_{11/2}$ state. These so-called erbium-ytterbium (Yb/Er) doped fibers are power scalable in that the higher absorption provided by the Yb-doping facilitates their use as cladding pumped fibers of moderate lengths. However, parasitic lasing at 1.06 $\mu$m typically limits the achievable

output power [21]. Furthermore, phosphorous codoping is required for efficient energy transfer, which reduces the gain bandwidth. These drawbacks of Yb/Er doped fibers have encouraged work on developing more efficient, Yb- and phosphorous-free amplifier and laser configurations, and have also motivated the theoretical work on broadband cladding-pumped L-band fiber amplifiers presented later in section 3.2 and in Publication I.

The ytterbium-ion has a simple electronic structure, with only one excited $^2F_{5/2}$ state manifold above the ground $^2F_{7/2}$ state within the optical spectral range of interest (from visible to NIR), as shown in Fig. 2.3(a). The excited state lifetime is typically $\sim$0.8 ms. The energy level structure of Yb allows distinctively different operational regimes depending on the pump and signal wavelengths [22]. Pumping can, in principle, be done in a broad range from 910 nm to 1064 nm, while gain can be realized at the 975 nm peak or at the secondary peak(s) starting from 1020 nm and reaching up to 1150 nm. The corresponding absorption and emission spectra are shown in Fig. 2.3(b). The large absorption cross-section, especially at the 976 nm peak, enables high pump absorption with short fiber lengths. With pump and signal wavelengths laying close to each other, the quantum defect is very small, only $\sim$8 % for 976 nm pumping. This allows scaling of output powers while maintaining significantly lower heat generation than with, for example, the erbium system. Slope power conversion efficiencies exceeding 80 % have been demonstrated [1]. The attributes discussed above make the Yb-ion especially well suited for power scaling purposes.

Finally, it is worth noting that rapid development in power scaling at 2 $\mu$m wavelength region has recently been demonstrated by using thulium doping. Thulium ion is conveniently pumped at 790 nm, and through a cross-relaxation process, two Tm-ions can be excited with a single pump photon. Slope efficiencies in the 50 % range have recently been demonstrated [23].

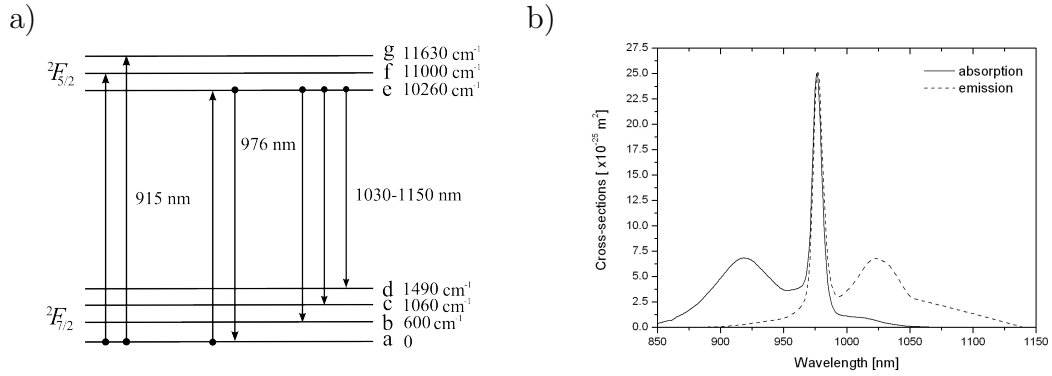


**Figure 2.3**: (a) Energy level diagram illustrating the ytterbium ground $^2F_{7/2}$ and excited $^2F_{5/2}$ state manifolds and possible transitions between the sub-levels and (b) absorption and emission cross-sections of ytterbium in aluminosilicate glass.

## 2.3 Dopant concentration

Increasing the doping concentration $N_c$ (in ions/m$^3$), and therefore also the core material absorption $\alpha$, increases the pump absorption and decreases the required fiber length linearly, without adversely affecting the overall fiber design (e.g. $D_{core}$, $D_{clad}$, $NA_{core}$). Higher doping concentration also means that the reservoir of stored energy will be higher. The resulting increase in $NA_{core}$, due to the RE-ion and other dopants used to increase the solubility, can largely be compensated for by the use of index-lowering dopants (such as fluorine). Therefore, from a purely power scaling perspective, there is no downside to increasing $N_c$. However, high doping concentration may lead to RE-ion clustering with resulting deleterious quenching processes which can seriously degrade the gain and efficiency of a laser or amplifier. The ytterbium-ion does not suffer from excited state absorption (ESA) processes or ion-to-ion energy transfer processes due to the simple electronic structure [24]. However, ion-pairs consisting of two Yb-ions are known to exhibit the effect of co-operative luminescence [25]. This effect requires two excited Yb-ions within close proximity, and produces a photon in the green (i.e. ∼500 nm) spectral range. While the green emission can be clearly observed with a naked eye in a well-pumped Yb-

fiber, this effect is too weak to significantly affect the gain [22]. Since the co-operative luminescence effect depends on the inversion and degree of clusterization (i.e. Yb-concentration), it has been proposed and used as a probe for clusterization and related effects, such as photodarkening [26],[27].

The photodarkening effect has been shown to be concentration-dependent [9],[28], and therefore poses a serious limitation on the achievable $N_c$. Ytterbium doping concentration of commercial ytterbium-fibers is currently at roughly $\sim 7.5 \cdot 10^{25}$ ions/m$^3$ (i.e. $\sim$1 wt-% Yb or $\alpha$=1000 dB/m at 976 nm) level. However, it is not yet clear whether this level is low enough for reliable long-term device operation. A much lower absorption level of 250 dB/m has been proposed as a safe, photodarkening-free doping level [29]. With ambiguity in the impact of photodarkening on the performance of an Yb-doped fiber laser or an amplifier, the approach usually adopted for limiting photodarkening is to reduce the Yb-doping concentration. However, reducing the doping concentration will adversely affect many applications that require short fiber lengths and it will limit the power scaling design options of double cladding fiber lasers. Therefore it is of utmost importance to improve the understanding of the photodarkening mechanism and to develop means for mitigating photodarkening without sacrificing the overall performance of the fiber laser/amplifier. This sets the motivation for the work presented in Publications II, III, IV, V, and VI.

It has been reported that in many ytterbium-doped fibers part of the Yb-ion population is quenched to a very short lifetime [30]. This effect manifests itself as a strong unsaturable loss with the same spectral shape as the absorption from the non-quenched ions. High concentration fibers with low level of quenching have been fabricated, although the mechanism of quenching was not identified. No pump-induced increase of loss was observed, suggesting a different mechanism to that which is involved in the photodarkening process [30].

In erbium-doped fibers, interactions between neighbouring Er-ions, such as the stepwise upconversion and the excitation migration, degrade the efficiency [31]. Furthermore, the process of excited state absorption, where an excited Er-ion in the metastable $^4I_{11/2}$-state manifold absorbs a pump or signal photon and is excited to yet a higher energy level, reduces the useful energy storage in the $^4I_{11/2}$-state and again results in reduction of overall efficiency [31]. These effects seriously limit the achievable doping concentration and hence pump absorption in erbium-doped fibers. Majority of commercially available erbium-doped fibers feature $\alpha$ at 980 nm in the 5 - 30 dB/m range.

## 2.4 Mode-filtering techniques

In a conventional SMF core design, the extractable energy is limited by the growth of ASE, which sets an upper limit to the achievable population inversion [10]. This limitation, and also those created by the threshold of the non-linear effects, may be alleviated by decreasing $NA_{core}$ and increasing $D_{core}$, which results in increased mode field diameter (MFD). This results in a smaller fraction of ASE being captured by the fundamental core mode (i.e. $LP_{01}$), and in a higher threshold for non-linear effects (which scale with the effective core area $A_{eff}$, e.g. $\propto D_{core}^2$). To maintain singlemode operation, increasing the core diameter requires subsequent decrease of $NA_{core}$ through the well known relation

$$V = \frac{\pi D_{core} NA_{core}}{\lambda}, \tag{2.4}$$

where $V$ is the normalized frequency and $\lambda$ is the wavelength. For a single-mode operation of a step-index fiber core, $V$ must satisfy the condition $V < 2.405$. However, $D_{core}$ cannot be increased indefinitely, as decreasing $NA_{core}$ results in an increasing bend sensitivity (e.g. losses) of the $LP_{01}$-mode. In practice, the lowest acceptable $NA_{core}$ is $\sim$0.06, resulting in a 12.5-$\mu$m upper limit on $D_{core}$ (at 1.06 $\mu$m). To go beyond this core diameter, one must find ways to deal with higher order modes

(HOM) which can extract significant portions of the stored energy and therefore degrade the output beam quality. Several techniques to extract the fundamental $LP_{01}$-mode from a multimode large-mode-area (LMA) fiber have been developed and can be categorized as:

1. Bend loss induced filtering of the HOMs
2. Preferential excitation of the $LP_{01}$-mode
3. $LP_{01}$-mode supporting refractive index/dopant designs

The bend loss method makes use of the fact that $LP_{01}$-mode is the least sensitive to bend loss and that the bend loss attenuation depends exponentially on the radius of curvature [32]. This method is practical to implement and has been demonstrated to provide excellent discrimination of the HOMs at least up to a V-value of 7.4 with a respective core diameter of 25 $\mu$m [7]. This method should be scalable to even larger core diameters, especially when used together with other methods for suppressing HOMs. An 80-$\mu$m core diameter double cladding fiber has been shown to provide a near diffraction-limited output beam quality with a 65-$\mu$m MFD using the bend loss method and the preferential excitation of the $LP_{01}$-mode [2]. However, 50-$\mu$m has been proposed as a practical limit for $D_{core}$, as bending-induced mode distortion severely impacts the effective mode area at larger core diameters [29]. Preferential excitation of the $LP_{01}$-mode is applicable with fibers having low mode coupling coefficient between the various modes so that if only the $LP_{01}$-mode is excited, it is able to propagate (and be amplified) through the active fiber core without significant coupling to the HOMs [6]. Single-mode femto-second pulse propagation over fiber lengths of tens of meters in a 50-$\mu$m diameter core fiber was demonstrated at 1.55 $\mu$m. Tapering of the active fiber has also been demonstrated to be a power scalable approach to achieving diffraction-limited output. Essentially a single-mode beam quality was demonstrated using an Yd-doped fiber with a 65-$\mu$m diameter core

at the output end and 11-$\mu$m at the narrow end [33]. A fundamental $LP_{01}$-mode selection may also be achieved through differential mode gain. This is done by optimization of the spatial active ion doping concentration in a way that provides preferential gain to the $LP_{01}$-mode [8]. Besides the above mentioned methods, a Chirally Coupled Core (CCC) fiber design is also listed in the fiber designs as being compatible with power scaling efforts [34]. Whichever method is used to reduce the HOM content, increasing $D_{core}$ has also the beneficial effect of increased core-to-cladding area ratio and therefore quadratically increased pump absorption. This is a very important design parameter, as it can be used, together with the dopant concentration, to control the length of the active fiber, therefore controlling the threshold at which non-linear effects come to play.

## 2.5 Fiber fabrication

Fabrication of RE-doped DCFs can be generally divided into three steps; fabrication of the core soot preform, fabrication of the fiber preform, and drawing of this preform to a fiber. The core soot preform fabrication methods can be categorized as being based on either hydrolysis or oxidation, referring to the specific chemical process used to produce the silica ($SiO_2$) particles [31]. In a hydrolysis-based process, $SiCl_4$ vapor is directed through the oxy-hydrogen flame, with $SiCl_4$ reacting with OH-groups created in the flame process. The produced silica particles are typically collected on a rotating mandrel. The produced soot is treated at high temperature to reduce the OH content of the glass. Fabrication processes based on hydrolysis are vapor axial deposition (VAD) [35], outside vapor deposition (OVD) [36] and direct nanoparticle deposition (DND) [37]. In an oxidation process, $SiCl_4$ reacts with oxygen inside a substrate tube. The reaction zone is heated from the outside of the tube typically with an oxy-hydrogen burner, which is traversed back and forth along the substrate tube to deposit a layer of silica inside the substrate tube. The modified chemical vapor deposition (MCVD) is based on an oxidation process

[35]. Within the two categories for producing the silica particles, there are several different techniques to incorporate the RE-ions (and the other codopants). Low vapor pressure of the RE-reactant (e.g. $ErCl_3$) requires placing the vapor source (i.e. RE-ion salt) close to the reaction zone, or bypassing this problem by using aerosols or higher vapor pressure organic compounds (e.g. chelates) [35], [38]. Vapor and aerosol delivery methods are, in principle, applicable to all the above mentioned fabrication processes mentioned above, but the use of chelates has been limited to MCVD. Solution doping of an MCVD produced soot preform is another method developed to overcome the problem of low reactant vapor pressure. The porous layer of silica inside the substrate tube is doped by filling the tube with a RE-chloride solution, and the solution is allowed to soak. The solution is then poured out, and the impregnated layer is dried at a high temperature with presence of chlorine (to remove water).

Following the fabrication of the core soot preform, i.e., deposition of the RE-ion and other codopants, the porous soot layer is sintered at high temperature to form a transparent glass [39]. The core and the substrate tube are then collapsed at high temperature to form a solid glass preform. Following this, the cladding is machined to a desired shape, after which the preform is ready for the drawing process. In the final drawing process, the glass preform is fed into a furnace placed at the top of a drawing tower. The furnace is heated to an appropriate temperature (between 1950-2200 °C) in order to melt the other end of the preform and to form a tip which begins to elongate the preform due to gravity. This tip is then directed through a series of rollers, which together with the furnace temperature and preform feed rate are used to control the outer diameter of the fiber. The fiber cools as it traverses down the drawing tower, and it is coated in-situ by being directed through a cup with the coating polymer and then through a UV-curing furnace. Finally, the coated fiber is spooled.

In comparison to fabrication of single-mode RE-ion doped fibers, DCFs with typ-

ically >10-$\mu$m-diameter and low $NA_{core}$ cores require both larger deposited core volumes and excellent control of the refractive index profile across the doped core. Although initially developed for manufacturing of small Er-doped single-mode fibers, the MCVD process combined with solution doping has shown versatility in meeting these requirements and is today widely used. In the DND process, the RE-ions and different index affecting constituents are doped in-situ, allowing continuous and accurate tailoring of the RIP [40]. This method has been shown to produce fibers with excellent mode behaviour [2] and high RE-ion concentration with a low clustering tendency [41]. As an outside deposition technology, DND is also scalable in the size of the soot preform.

## 2.6 State-of-the-art and fundamental limitations

Owing to the double cladding fiber structure, the large-mode-area core design, and the development of reliable high-power pump diode sources, tremendous increases in output power have been achieved over a short period of time. A review of power evolution of state-of-the-art diffraction limited fiber lasers was pusblished by Limpert *et al.* [42] in 2007. For Yb-doped fibers, the highest demonstrated continuous wave power today is 3 kW [1]. At the eye-safe wavelengths, the power scaling efforts so far have largely been focused on the Er/Yb co-doped fibers with a record of 188 W of cw power at 1.57 $\mu$m [21]. Another approach to power scaling at 1.5 $\mu$m is to resonantly cladding pump (i.e. at 1.53 $\mu$m) an erbium-doped double cladding fiber [43]. With this approach, power scaling to ∼100 W output power regime at 1.59 $\mu$m has been demonstrated with ∼60 % optical-to-optical power conversion efficiency [44]. Impressive results have recently also been demonstrated using a thulium-doped LMA fiber with ∼64 % slope efficiency and 300 W cw output power demonstrated at 2.0 $\mu$m [23].

The ultimate power-scaling limits for fiber lasers and amplifiers are governed by

thermal effects, non-linearities, the end-facet damage threshold and the brightness of the pump diodes [45],[29]. Heat generated due to a quantum defect can lead to coating damage, fiber fracture or even melting of the core [46]. Fraction of the pump power converted to heat can conservatively be assumed to be in 10-15 % range for a high efficiency fiber, which means heat generation of ∼150 W per kilowatt of optical output power. This heat load can be distributed over the length of the active fiber, and therefore be efficiently cooled using appropriate heat-sinking. Keeping the fiber temperature well below 100 °C also minimizes the risk of coating damage. The stress fracture limit for a 50-m long fiber was found to be 7.56 MW, indicating an extractable power of 1.5 kW/cm [46]. Therefore, a thermally-induced fracture is improbable even in multi-kW power regime. However, thermal lensing, i.e., guiding by the heat-induced temperature gradient, is considered to impose a limitation on the achievable output power [29].

The main non-linear limitations in power scaling are imposed by stimulated Raman scattering (SRS) and stimulated Brillouin scattering (SBS). The SRS causes power of the propagating signal to be downshifted in frequency (by ∼13 THz) due to interaction with optical phonons. The SBS also results in frequency downshift of the incident beam, but in the opposite direction to the propagation of the original signal. Also, the frequency shift in the SBS is much smaller (∼10 GHz) compared to that occurring in the SRS. SRS threshold power can be approximated by [47]

$$P_{th}^{SRS} \cong \frac{16 A_{eff}}{g_R L_{eff}}, \tag{2.5}$$

where $A_{eff}$ is the effective core area, $g_R$ is the Raman peak gain coefficient ($1{\cdot}10^{-13}$ m/W in fused silica at 1 $\mu$m), and $L_{eff}$ is the effective fiber length, accounting for gain or loss in the fiber. Similar equation may be derived for the SBS threshold as

$$P_{th}^{SBS} \cong \frac{21 A_{eff}}{g_B L_{eff}}, \tag{2.6}$$

where $g_B$ is the Brillouin gain coefficient ($5{\cdot}10^{-11}$ m/W in fused silica at 1 $\mu$m). The impact of the SBS in a CW fiber laser system will strongly depend on the

amplified spectral bandwidth. The SBS is therefore a performance limiting factor mainly in single-frequency fiber lasers, whereas the SRS limits the power scaling of more typical, spectrally broadband high-power fiber lasers. In pulsed fiber lasers and amplifiers, non-linear effect of self-phase modulation (SPM) may also impose a limit on achievable pulse energy due to pulse broadening [47].

Bulk damage threshold for silica in the ns pulse regime is $\sim$5000 W/$\mu$m$^2$ [48]. However, in fibers the damage effect is usually observed at the end facet. The end-facet continuous wave damage threshold of $\sim$10 W/$\mu$m$^2$ has been derived from experimental data [49]. While this is two orders of magnitude lower than for the bulk (in pulsed regime), it allows operation in multi-kW regime through the use of large MFD fibers or/and mode field expanding end caps. The theoretical power scaling limit of a diffraction limited single fiber laser or a MOPA system, taking into account all the above mentioned effects and also the pump diode brightness, was found to be 36 kW for broadband fiber lasers, under the assumption of an unrestricted MFD [29]. Scalability of the MFD may limit the power to around 10 kW.

# 3 Modeling of double cladding fibers

Modeling of erbium- and ytterbium-doped double cladding fibers can conveniently and accurately be done by using propagation and rate equations of a homogeneously broadened, two-level laser system [50],[22]. As the lifetime of the pump excited $^4I_{11/2}$ state in erbium is very short and the transition to the $^4I_{13/2}$ state is non-radiative, this system can be reduced to a two-level system [50]. Further, resonant (i.e. signal transition) pumping of both erbium (e.g 1480 nm) and ytterbium (e.g. 976 nm) can also be treated as a two level-system due to a rapid thermalization in the ground and excited state manifolds. Within the two-level laser system approximation, the complexity of the models varies from full numerical spatial-mode modeling of amplified spontaneous emission [51] to analytic solutions of arbitrary number of pump and signal beams, but the models neglect the saturation effect of the ASE [52]. The model described here and used in Publications I and III is based on the full-numerical spatial mode model [51]. The normalized local upper ($N_2$) and lower ($N_1$) state populations of a two-level energy system are governed by the rate equations

$$\frac{dN_2}{dt} = (R_{12} + W_{12})\, N_1 - (R_{21} + W_{21} + A_{21})\, N_2 \tag{3.1}$$

$$\frac{dN_1}{dt} = -(R_{12} + W_{12})\, N_1 + (R_{21} + W_{21} + A_{21})\, N_2, \tag{3.2}$$

where $R$ is the pump transition, $W$ is the signal (and ASE) transition and $A_{21}$ is the spontaneous emission transition rate coefficient. In steady-state, these equations are reduced to

$$N_2 = \frac{R_{12} + W_{12}}{R_{12} + W_{12} + R_{21} + W_{21} + A_{21}} \tag{3.3}$$

$$N_1 = 1 - N_2. \tag{3.4}$$

The various transition rates are given by

$$R_{12,21} = \sigma_{a,e}(\nu_p)\frac{I_p}{h\nu_p} \tag{3.5}$$

$$W_{12,21} = \sum_k \sigma_{a,e}(\nu_k)\frac{I_k}{h\nu_k} \tag{3.6}$$

$$A_{21} = \frac{1}{\tau_{21}}, \tag{3.7}$$

where $\sigma_a$ and $\sigma_e$ are the absorption and emission cross-sections, and $\nu_p$ and $\nu_k$ are the pump and signal/ASE frequencies, respectively. Index $k$ is used to account for more than one narrowband signal beam and broadband ASE by summing up k frequencies with $\Delta_{ASE}$ bandwidth resolution. $I_p$ and $I_k$ are the pump and signal intensities and $\tau_{21}$ is the fluorescent lifetime of the excited state. For a double cladding fiber $I_p = P_p/A_{clad}$, where $P_p$ is the pump power (in W) [53]. The normalized mode profile $\psi_n(r)$ of the core-propagating fundamental mode (i.e. $LP_{01}$) is derived through the Bessel functions. The signal (and ASE) intensity distribution is then given by $I_k(z,r) = P_k(z)\psi_n(r)$, implying that the dependence on z and r is implicit also in the definitions of $N_{1,2}$ and the various transition rates. The local gain and absorption coefficients are given by

$$\gamma_e(\nu_{k,p}, z) = 2\pi\sigma_e(\nu_{k,p})N_c \int_0^a N_2(r,z)\psi_n^{k,p}(r)dr \tag{3.8}$$

$$\gamma_a(\nu_{k,p}, z) = 2\pi\sigma_a(\nu_{k,p})N_c \int_0^a N_1(r,z)\psi_n^{k,p}(r)dr, \tag{3.9}$$

where the integral term gives the overlap of the signal/ASE mode with the distribution of ions in the doped core with a radius $a$. Using these coefficients, the propagation of signal, ASE and pump can be written as

$$\frac{dP_k}{dz} = u_k\gamma_e(\nu_k, z)\left[P_k(z) + 2h\nu_k\Delta\nu_{ASE}\right] - u_k\gamma_a(\nu_k, z)P_k(z) \tag{3.10}$$

$$\frac{dP_p}{dz} = u_p\left[\gamma_e(\nu_p, z) - \gamma_a(\nu_p, z)\right]P_p(z) \tag{3.11}$$

where $u_k$ is used to specify whether the signal is propagating in forward ($u_k$ = 1) or backward ($u_k$ = -1) direction. The second term in parenthesis in Eq. 3.10 accounts for the creation of spontaneous emission, i.e. noise. For lossy fibers a background loss parameter $\alpha_{BG}$ is added to the above equations. These equations requires numerical solving, since the forward and backward ASE distributions and their contributions to the local inversion are not known *a priori*. The relaxation method uses an iterative procedure, where the propagation equation is iterated back and forth until a self-consistent solution satisfying the boundary conditions is found [19].

## 3.1 Inversion and ASE in cladding-pumped fiber amplifiers

In Publication I, propagation of the ASE and the resulting longitudinal inversion distribution was simulated in a cladding pumped erbium-doped fiber amplifier. Cladding-pumped EDFAs have been proposed to alleviate the bottleneck of low saturated output powers associated with conventional singlemode diode pumped L-band amplifiers [54], [55]. L-band refers to the long-wavelength optical communication window between 1565 nm and 1625 nm. The emission cross-section of erbium extends to this wavelength range, but the gain coefficient is much lower than at the 1.53 $\mu$m gain peak. To avoid gain build-up at 1.53 $\mu$m, L-band EDFAs must be operated in relatively low average inversion level of $\sim$35 % [56]. Therefore, up to 200-m long fibers are required to achieve gains comparable to EDFAs operating in the conventional 1530 nm to 1565 nm band [57]. Singlemode diode pumping at 980 nm results in high inversion and gain at the pump input end, and the resulting high counter-propagating ASE power reduces the amplifier efficiency. Detuning the pump away from the 980 nm absorption peak has been proposed for a more uniform pump distribution [58]. In cladding-pumping, the distribution of pump is inherently more uniform along the length of the fiber. Increasing the pump cladding area reduces the pump absorption according to Eq. 2.2, resulting in more uniform absorption of pump power along the fiber length. This in turn was simulated to result in a more uniform inversion distribution along the fiber length, as shown in Fig. 3.1(a). As a result, the build-up of short-wavelength (i.e. 1.53 $\mu$m) gain and ASE was reduced, leading to a more efficient amplification in the 1.6 $\mu$m region. Optimization of the quantum conversion efficiency (QCE), i.e.

$$QCE = \frac{\lambda_s}{\lambda_p} \frac{P_s^{out} - P_s^{in}}{P_p^{in}}, \tag{3.12}$$

was determined to involve a trade-off between more uniform pump absorption leading to a more efficient extraction of signal power and increase of redundant (i.e. unabsorbed) pump power, as illustrated in Fig. 3.1(b). A 26 dBm output power, Yb-free and fully integrated cladding-pumped L-band EDFA was demonstrated by

Bousselet *et al.* [54]. Flat gain of 34 dB and a noise figure of about 8 dB was measured across 1570-1603 nm with -9 dBm input signal power and 1.76 W of launched pump power.

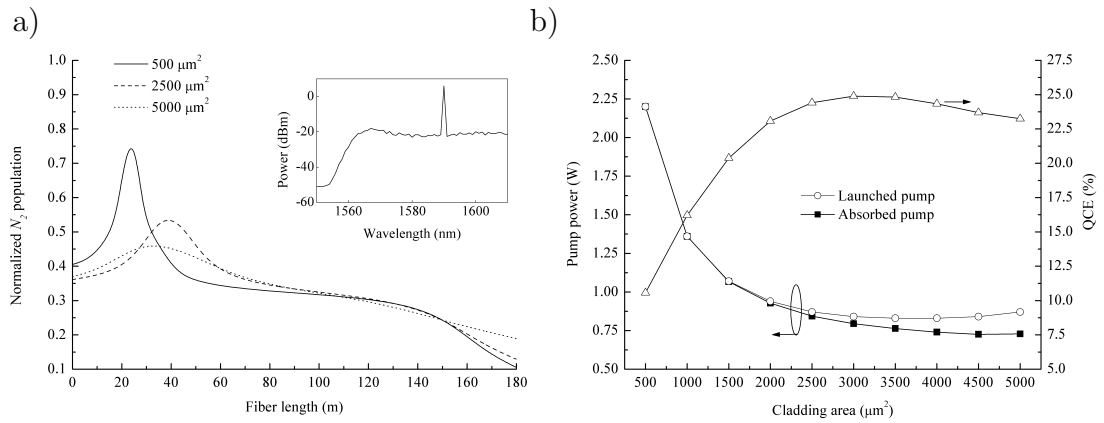


**Figure 3.1**: (a) Variation of longitudinal inversion distribution in a cladding pumped erbium-doped fiber with different cladding areas. Inset graph presents the simulated output spectrum for the 20-dB-gain EDFA with 500 $\mu$m$^2$ cladding area and b) launched and absorbed pump power and QCE as a function of cladding area. Gain is fixed at 20 dB for a 0-dBm signal at 1590 nm by varying the pump power (Publication I).

In Publication III, cladding pumping was used to produce a controllable, longitudinally and transversally uniform inversion in an Yb-doped fiber sample, as illustrated in Fig 3.2. In a short (i.e. $< 10$ cm), cladding-pumped sample the normalized inversion $N_2$ is well approximated by

$$N_2 = \frac{\sigma_a(\nu_p)}{\sigma_a(\nu_p) + \sigma_e(\nu_p)} \frac{1}{1 + I_{sat}/I_p}, \tag{3.13}$$

which was derived using equations (3.3)-(3.7) with $W_{12,21}$=0 (i.e. no ASE) and substitution $I_{sat} = h\nu_p / \left[(\sigma_a(\nu_p) + \sigma_e(\nu_p))\tau\right]$. Hence the inversion can be controlled by the pump power with the maximum inversion limited by the cross-sections at the pump wavelength. A thorough study on inversion distributions in short Yb-doped fibers with different pumping configurations was published by Koponen *et al.* [59].

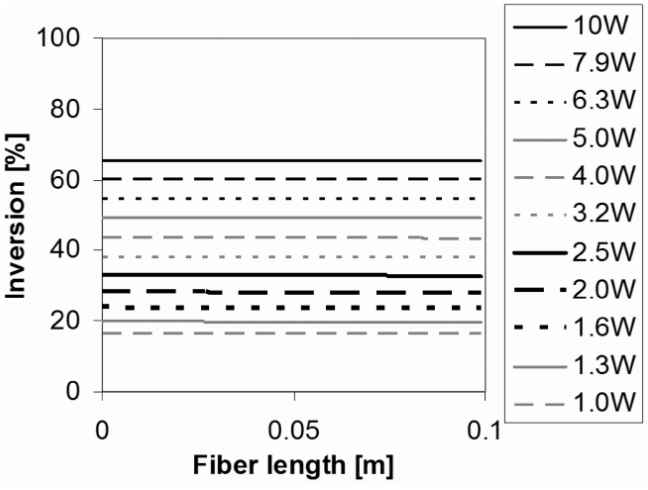


**Figure 3.2**: Longitudinal inversion profile of a 10-cm long Yb-doped fiber sample cladding pumped at 915 nm with different pump powers (Publication III).

# 4 Photodarkening effect in ytterbium-doped fibers

Photodarkening commonly refers to irradiation-induced increase of the material absorption or scattering over time. Its mechanism and characteristics may vary greatly with material. In many cases, the mechanism is attributed to the formation of light absorbing color centers [60]. A color center refers to a trapped charge, i.e. an electron or a hole, which is trapped by some defect within the glass matrix. Free charges are generated, for example, when an ion is excited to energies overlapping with the conduction band or charge-transfer states, therefore transferring an electron to or from a nearby ligand (i.e. photoionization). The excitation is typically produced by an intense optical radiation in the UV-wavelength range, but may also take place as a multi-photon absorption or a stepwise upconversion process [60],[61]. A light-induced refractive index change in RE-doped fibers has been studied within the context of achieving permanent fiber Bragg gratings. Exposing $Ce^{3+}$, $Pr^{3+}$- or $Eu^{2+}$-doped silicate glasses to UV light with wavelength matching specific electronic transitions of the ion was shown to lead to permanent RI and absorption coefficient changes over a broad spectral range [62],[63]. A thulium-doped fiber was observed to exhibit permanent photodarkening when exposed to a moderate-power 1064-nm radiation, with the initial rate of photodarkening showing approximately fifth-order power dependence [61]. Photodarkening in a $Tb^{3+}$-doped fiber under 488-nm light was attributed to a three-photon process and photoionization of $Tb^{3+}$ [64].

In Publication II and in preceding conference papers [9],[65], photodarkening was observed in Yb-doped fibers under 975 nm pump excitation. A short sample of a singlemode aluminosilicate ytterbium-doped fiber was pumped with roughly 300 mW of pump at 974 nm to produce a high and uniform inversion, and the transmission spectra were recorded before and after irradiation. The obtained photodarkening-induced excess loss spectra indicated nearly exponential growth of loss towards the shorter wavelengths in the 600-1100 nm wavelength range, as shown in Fig. 4.1(a).

Using data from 22 different fibers, the induced loss at 633 nm was determined to be 71 times higher than at signal wavelengths between 1040-1070 nm, as shown in Fig. 4.1. Mattson *et al.* observed roughly half of the 30 studied microstructured Yb-fibers to agree with the ratio of 71 between 633 nm and 1060 nm [66]. Differences in the ratio were explained in terms of the presence of different color centers and their dependence on the core composition. The dependence of photodarkening

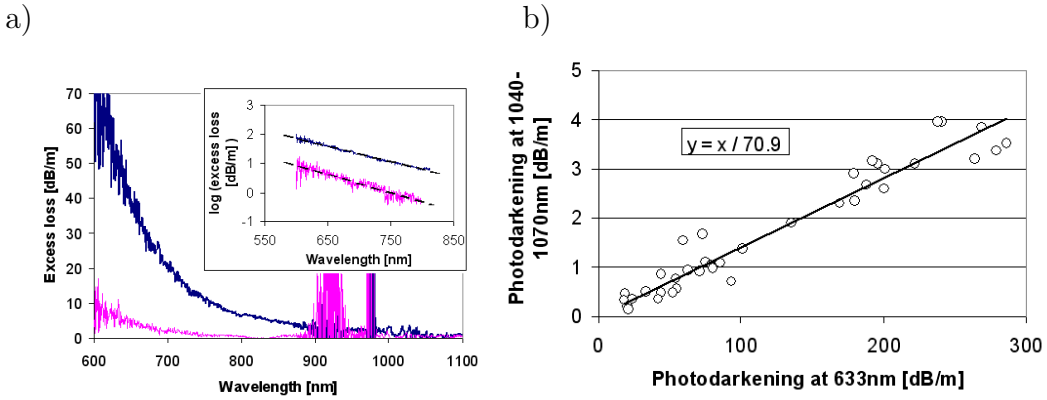


**Figure 4.1**: (a) Spectral shape of photodarkening-induced loss for two fibers with different composition and (b) relation between the 633 nm and 1040-1070 nm losses, measured from fibers covering 22 different glass compositions (Publication II).

on the pump wavelength was studied by Kitabayshi *et al.* [67], who photodarkened fibers using pump diodes with different wavelengths (i.e. 940, 976, and 1150 nm) having the same 100-mW power. It was concluded from the induced loss spectra that photodarkening is not driven by the pump power, but rather, by the density of excited ytterbium-ions.

Temporal and spectral evolution of photodarkening was studied in detail by Manek-Hönninger *et al.* [68]. The development of the absorption spectrum in the visible and IR wavelengths (from 300 nm to 1200 nm) was measured versus progressive cladding pumping with 45 W at 976 nm. The peak of absorption losses was shown to be located in visible/UV wavelengths. The impact of progressive photodarkening on lasing properties of a CW fiber laser was studied by sequentially suppressing

laser oscillations by blocking a high reflective mirror in the laser cavity, therefore accelerating photodarkening. Considerable decrease of slope efficiency was observed with a longer exposure of the fiber to the "accelerated photodarkening" condition, establishing a relation between photodarkening and efficiency reduction. Morasse *et al.* compared the temporal degradation of a 20 W cladding-pumped fiber laser and a 60 mW core-pumped amplifier [28]. The normalized output power of the core-pumped amplifier degraded by as much as 80 % within the first 2 hours of operation, while the cladding-pumped fiber laser's output power remained unchanged. The difference in output power stability was again attributed to differences in the inversion distributions of the two configurations, with high inversion in the core pumped amplifier proposed to be responsible for the observed rapid degradation.

## 4.1 Inversion dependence

A quantifiable measurement method for derivation of the photodarkening rate dependence on inversion was established in Publication III and in a preceding conference paper [69]. The progress of photodarkening was measured at different inversion levels by monitoring a probe at 633 nm, launched into the Yb-doped aluminosilicate fiber sample core through a multimode combiner together with the pump light from fiber coupled pump diodes operating at ∼920 nm. A strong dependence of the rate of change of normalized transmittance at 633 nm on the inversion level was observed, as shown in Fig. 4.2(a), identifying inversion as a key controlling variable. A bi-exponential fit to the data was used to obtain the rate constants, which were then plotted agains the respective simulated inversion levels using a log scale on both x- and y-axes. This plot, shown in Fig. 4.2(b), indicated approximately seventh-order dependence on inversion. It was concluded that photodarkening rate is proportional to $[Yb^*]^7$ (where $Yb^*=N_2N_c$ is the excited Yb-ion density in ions/m$^3$), suggesting that seven excited Yb-ions in close proximity may be involved in the photodarkening process. Similar results were presented by Shubin *et al.* [70], who derived a

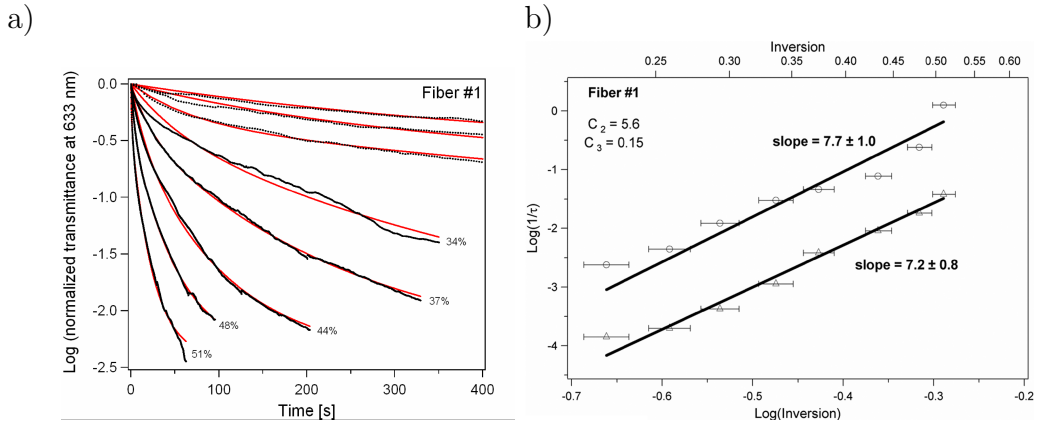


**Figure 4.2**: (a) Photodarkening decay curves measured at varying inversion levels and (b) photodarkening rate constants as a function of inversion (Publication III).

sixth-order dependence on inversion. A stretched-exponential function was used in this case to extract the rate constants from the various decay curves. Photodarkening rate dependence of $[Yb^*]^{3.5}$ was derived by Jetschke *et al.* [71], indicating an involvement of 3-4 excited Yb-ions in the photodarkening process. Similar experimental measurement arrangement as in [69] was used, but a lock-in technique was utilized to improve the probe light detection sensitivity. A systematic source of error in the use of the stretched-exponential function was studied in [72]. Rate constants were observed to depend on the measurement length if the measurement time was too short. Using the presented guidelines, a rate dependence of $[Yb^*]^{4.3\pm0.5}$ was found for a typical aluminosilicate fiber. Since the measurement duration for low-photodarkening level fibers and/or low inversion levels can be extremely long, accelerating photodarkening measurements by heating the fiber was proposed by Leich *et al.* [73].

## 4.2 Defect mechanism

Several theories have been put forward to explain the photochemical mechanism behind photodarkening in ytterbium-doped fibers. Jasapara *et al.* proposed that photodarkening is caused by a reduction process, where $Yb^{3+}$ converts to $Yb^{2+}$ through a capture of excited electrons by $Yb^{3+}$ pairs [74]. Along the same lines, Guzman Chávez observed a reduction of 977-nm absorption with progressive photodarkening, assigning the change to an $Yb^{3+} \longrightarrow Yb^{2+}$ conversion [75]. Interestingly, the 977-nm absorption coefficient started to recover after ∼100 minutes of irradiation, and recovered to nearly the initial level after 300 minutes, even though the induced losses at visible wavelength were continuously increasing. Engholm *et al.* observed a strong absorption band in the UV range (∼230 nm) for Yb-doped aluminosilicate glass, and attributed this absorption to charge transfer (CT) transitions [76]. Excitation into this CT band was hypothesized to involve a temporary formation of an $Yb^{2+}$-ion and a bound hole. Excitation into a higher lying CT band (at ∼180 nm) was shown later in [77] to correlate with the induced visible losses, providing strong evidence of the involvement of charge transfer transitions in the photodarkening process. Yoo *et al.* assigned the UV range absorption near 230 nm to an ytterbium-related oxygen deficiency center (ODC), and observed photodarkening using 488-nm excitation and two-photon absorption [78]. They supported their hypothesis with measurement of oxygen loaded fibers showing reduced photodarkening. The origin of the UV range absorptions is still under debate [79],[80]. Different hypotheses on the excitation mechanism to reach UV absorption energies have also been proposed, involving Yb-ion pairs acting as intermediate energy states and multi-photon absorption from an Yb-ion excited state [75],[77], but conclusive evidence supporting one particular mechanism has yet to be presented. Recently, Arai *et al.* studied photodarkening in aluminosilicate fibers using electron spin resonance (EPR) measurement [81]. Fiber samples irradiated with 976 nm and bulk samples exposed to gamma-ray irradiation both indicated a presence of aluminum-oxygen hole centers (Al-OHC). The optical absorption spectrum of a gamma-ray irradiated bulk glass

sample exhibited a maximum at 350-400 nm. The deconvolution of this spectrum indicated a presence of three loss centers, located at 302 nm (Al-E' center), 388 nm (Al-OHC) and 539 nm (AL-OHC). Therefore, photodarkening loss in NIR was attributed mainly to the presence of Al-OHCs.

## 4.3 Photo-bleaching

Photo-bleaching of induced losses was observed by Manek-Hönninger *et al.* [68]. A short exposure time to UV light at 355 nm with pulse energy of $\sim$90 $\mu$W was reported to recover the absorption spectrum to nearly the pre-photodarkened state. Further, lasing properties of the photo-bleached fiber indicated the same slope efficiency as with an unphotodarkend pristine fiber, even after going through several cycles of consecutive photodarkening and photo-bleaching. Photo-bleaching was also reported by Guzman Chávez *et al.* using 1 mW of green (543-nm) irradiation for 1 hour [75]. The induced photodarkening loss was partially removed by this exposure. Evidence of equilibrium photodarkening states depending on the pump power was presented by Jetscke *et al.* [71]. Upon reaching nearly the saturation of photodarkening at a given pump power, reducing the pump power to a lower level was shown to result in a reduction of the induced loss. An equilibrium loss level could be reached using samples with different initial conditions (one pristine, the other photodarkened) pumped with the same pump power. The reduction of the loss was assigned to a pump-induced photo-bleaching. Further, the equilibrium loss level was shown to depend on the inversion level.

## 4.4 Mitigation

Reduction the photodarkening effect by increasing the aluminium co-doping was presented by Kitabayashi *et al.* [67]. The increase of aluminum concentration from 0.5 wt-% to 3.0 wt-% reduced the induced losses at 800 nm to one-fourth, which was attributed to reduced Yb-ion clustering. Morasse *et al.* showed that the induced losses at 1100 nm depend linearly on the Yb-ion concentration beyond a threshold concentration of about $5 \cdot 10^{25}$ ions/m$^3$ [28]. Increasing aluminum co-doping was also used by Morasse to engineer fibers for lower photodarkening. Engholm *et al.* showed that hydrogen-loading of an Yb-fiber in a pressure chamber at room temperature resulted in a significant reduction of the induced loss at 600 nm [77]. The improvement in photodarkening resistivity was assigned to $H_2$-molecules reacting with the holes on the oxygen atoms, strongly suppressing the formation of the hole related color centers. A thorough study on optimization of core composition with regards to photodarkening and the lasing efficiency was published by Jetschke *et al.* [82]. Core composition with equal content of aluminum and phosphorous was found to be the most promising candidate to achieve Yb-doped fibers with low photodarkening, high laser efficiency and low numerical aperture. Co-doping with cerium was found to greatly improve the photodarkening resistance of aluminosilicate Yb-doped fibers, owing to the electron- and hole-trapping property of the cerium-ion [83]. However, cerium doping increases $NA_{core}$, which may limit the applicability of this approach in some LMA designs.

## 4.5 Modeling

Currently, there is no comprehensive model of photodarkening able to predict the lifetime of Yb-doped fiber devices exists, as the photochemical mechanism remains largely unexplained. However, several semi-empirical models have recently been

developed in an effort to improve the understanding of the joint effects of photo-darkening and bleaching in Yb-doped fibers [66],[84],[85].

# 5 Thermodynamic analysis of photodarkening

Thermodynamic analysis can be used to identify different mechanisms and their equilibrium states by their activation temperature or energy. In the case of kinetic data, multiple photochemical reaction mechanisms result in a multi-exponential decay of absorption as a function of time, which is difficult to analyze and cannot be tied to specific physical mechanisms. Furthermore, thermodynamic data can be put on an absolute scale (such as eV) without detailed information about fiber parameters, such as the rare-earth dopant density. Thermal bleaching of photodarkening was first published by Jasapara *et al.* [74]. An aluminosilicate fiber sample ($L$=18 cm) was photodarkened for 25 minutes using 300 mW of pump at 976 nm. A complete recovery of the fiber absorption spectrum to the pre-photodarkened state was observed when heating the fiber to 500 °C. Transmission at 620 nm as a function of furnace temperature indicated a smooth, continuously decreasing behaviour of the induced loss. It was concluded that thermal energy of the order $k_BT$=0.07 eV was needed to completely reverse the darkening mechanism. Almost a complete thermal bleaching of photodarkening at 400 °C was observed by Shubin *et al.* [70]. A change in the heating rate growth from 0.15 °C/s to 1 °C/s was not observed to lead to significant changes in the bleaching dynamics. This chapter gives an overview of the thermal bleaching experiments and results presented in Publications IV and V. This research has been carried out using commercial 20-$\mu$m diameter core, low numerical aperture double cladding LMA fibers from two different suppliers.

## 5.1 Thermal ramp-up/down cycling measurement

In Publication IV, thermal bleaching of photodarkening was studied by applying triangular thermal ramp-up/down cycles to a photodarkened aluminosilicate fiber sample using the measurement setup presented in Fig. 5.1. A key feature of the ap-

plied measurement approach was that the same sample was thermally recovered to its pre-photodarkened state by applying a high temperature "annealing" step, allowing repeated analyses without measurement errors related to changing of the sample (e.g. sample length and doping consistency) [86]. A sequence of photodarkening

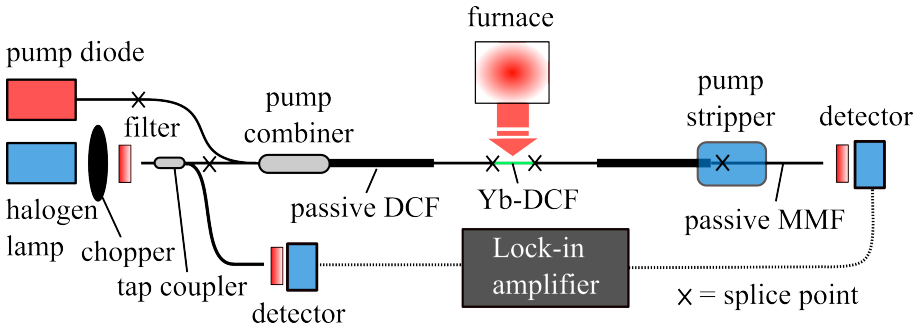


**Figure 5.1**: Experimental setup for measuring photodarkening and thermal bleaching of induced losses.

and thermal bleaching was first recorded at 600 nm. The sample was then thermally recovered and the same sequence was repeated with a measurement wavelength of 670 nm. To compare the two results, spectral loss ratio between 600 nm and 670 nm was assumed to be constant 1.98 (taken from a room temperature loss spectra shown later in Fig. 5.3) and the 600 nm data was scaled with this ratio. Results of these measurements are shown in Fig. 5.2(a)-(b). Two important observations were made from these graphs:

1. The two curves overlap only at room temperature, i.e., at the end of photodarkening measurement(a)/beginning of thermal bleaching (b). The deviation between the data sets appears to correlate with temperature (b).

2. Prior to the initiation of thermal bleaching, further heat-induced increase of loss takes effect (b).

The observed heat-induced increase of loss was measured to be permanent by applying a thermal cycle to 325 °C and back to room temperature (RT). Loss spectra measured after the irradiation and after causing the heat-induced increase of loss (i.e. darkening) are presented in Fig. 5.3. The post-irradiation heat-induced darkening was estimated to constitute to roughly 20 % of the total induced losses. Similarity of the spectral shapes indicated that the heat-induced darkening originates from the same type of color center as is created through the NIR excitation route. Figure 5.3 also presents two photodarkening spectra measured at elevated temperatures (i.e. 148 C and 304 C). From these graphs, the deviation between 600 nm and 670 nm measurement wavelengths can be identified as the spectral broadening of the induced loss spectrum. The 600 nm measurement wavelength is very close to the cross-over wavelength $\lambda_0$=612 nm, where the temperature dependence is negligible. Wavelengths shorter than $\lambda_0$ can be seen to exhibit decreasing losses, while wavelengths longer than $\lambda_0$ (such as 670 nm) exhibit increased losses with increasing temperature. The magnitude of the change $d(\Delta\alpha)/dT$ is proportional to $|\lambda\text{-}\lambda_0|$ and is 0.19 (dB/m)/ °C at 670 nm for the measurement in question. The relative change of loss increases with wavelengths above $\lambda_0$ and is estimated to be ∼0.5 %/ °C at the 915 nm pump wavelength. Gaussian fits to the experimental data indicate that the observed temperature-dependent spectral changes in the 550-850 nm wavelength range are well described by the spectral broadening of a single absorbing species.

Previous publications on thermal bleaching of photodarkening [74],[70] do not report on post-irradiation increase of loss. This may be due to differences in the experimental configurations or in the composition and properties of the studied fibers. Shubin *et al.* used a short, 500 nm probe wavelength, which may result in the temperature dependence of the loss spectrum compensating for the heat-induced darkening. However, Sahu *et al.* observed a room temperature post-irradiation temporal loss growth at 1.28 $\mu$m of a 488-nm irradiated aluminosilicate fiber over a time period of 3 days at room temperature [87]. The fiber length used in this experiment was 10 meters. In a recent publication by the same group, this effect was again observed

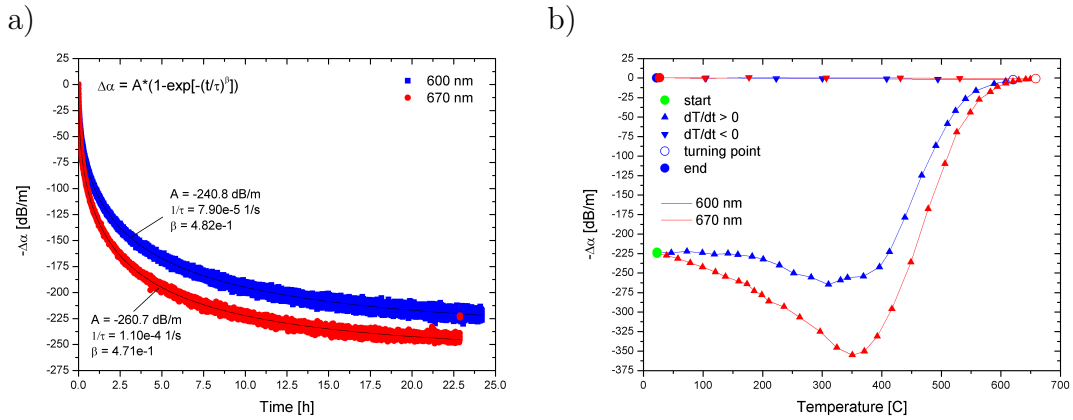


**Figure 5.2**: (a) Photodarkening-induced fiber absorption coefficient change $\Delta\alpha$ at 670 nm (red circles) and 600 nm data converted to the same scale as the 670 nm by dividing by 1.98 (blue squares) and (b) thermal bleaching of induced losses (Publication IV).

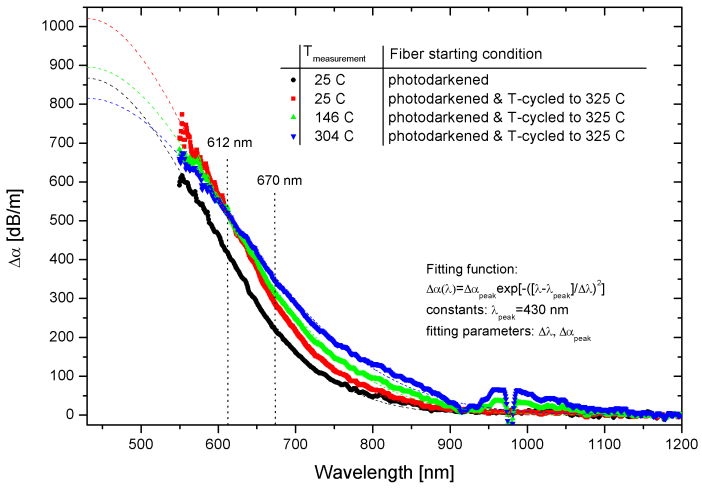


**Figure 5.3**: Absorption coefficient change spectra $\Delta\alpha(\lambda)$ measured after photodarkening, after thermal cycling (from RT to 325 °C and back), and at 146 °C and 304 °C after completing the first thermal cycling sequence (Publication IV). Dashed lines show a Gaussian fit to the respective data sets.

in a 2-m long Yb-doped aluminosilicate fiber even at room temperature, and was seen to be enhanced by increasing the fiber temperature to 120 °C [88]. A quantitative comparison of these results to those presented in Publication IV is difficult due to differences in the experiments (e.g. excitation wavelength and fiber length). In a recent paper by Leich *et al.*, thermal broadening of the induced loss spectrum was also reported [89]. The increase of loss was observed at 633 nm when increasing the temperature from room temperature to ∼230 °C, after which the losses begun reducing (i.e. bleaching). This result is in qualitative agreement with the data presented in Fig. 5.2(b). The difference in the temperatures (of ∼100 °C) in which the recovery is initiated and at which full recovery is reached, can probably be attributed to differences in fiber compositions. However, the permanency of the thermally-induced loss was not studied in [89], and therefore the presented results are likely to include the effect of the post-irradiation heat-induced darkening.

For the spectral broadening to explain also the ∼20 dB/m step observed in the 670 nm data in Fig. 5.2(a), the fiber core temperature was estimated to be ∼120 C when the pump was turned on. Based on an estimate of the amount of pump light absorbed by the fiber sample (∼270 mW) and the quantum defect for pumping at 915 nm, an increase of the core temperature of this magnitude was not predicted. This discrepancy is addressed in section 5.3, where a measurement of the fiber temperature during photodarkening is presented.

## 5.2 Thermal activation energy

In Publication V and in a preceding conference paper [90], the activation energy of the photodarkening-induced defects was measured using an isothermal measurement method. This method is based on work by Erdogan *et al.* on predicting the post-irradiation thermal decay of fiber Bragg gratings (FBGs) [91]. Erdogan developed a model to explain the observed time-dependent decay of the induced

index-change as a thermal decay from a distribution of trap sites. This so-called master/demarcation energy curve approach has also been applied to analyze the recovery in radiation-induced loss in Er-Yb doped silica fibers [92]. While the excitation mechanism in photodarkening is different from that used in writing FBGs (i.e. NIR vrs UV-excitation), the glass host material used is roughly the same, and therefore, the defects created were hypothesized to similarly occupy a distribution of trap sites of different energy-well depths. A typical isothermal measurement cycle applied in Publication V is illustrated in Fig. 5.4(a). An Yb-doped fiber sample ($L$=5 mm) is first photodarkened until the loss is fully saturated. For the duration of this measurement, the sample is held uncoated in air, and forced air cooling is applied to the sample. The fiber temperature is then increased (as a step-function) using a pre-heated furnace and the recovery curve is recorded. The previously mentioned heat-induced increase of loss is first observed. The following initially fast recovery slows down considerably with passing time. At the end of the measurement, fiber temperature is further increased to recover the sample completely. Figure 5.4(b) shows three such isothermal bleaching measurements taken at different temperatures. Each data set has been normalized with $\alpha_{max}$. The experimental data is very well described by a function of form

$$\Delta\alpha_n(t) = \frac{1}{1 + (t/\tau)^{\beta}}, \tag{5.1}$$

where $\tau$ is a time constant (in seconds) and $\beta$ is a dimensionless power-law exponent. From the best-fit parameters in Fig. 5.4(b), $\tau$ was found to be an exponential function of temperature while $\beta$ exhibited a linear dependence on temperature. Central to the applied theoretical picture is the assumption that the (post-irradiation) population of the trap sites as a function of temperature and time is uniquely determined by a "demarcation energy" ($E_d$), given by

$$E_d = k_B T ln(\nu_0 t), \tag{5.2}$$

where $k_B$=8.617 $\cdot$ $10^{-5}$ eV/K is the Boltzmann constant, and the parameter $\nu_0$ represents the characteristic vibrational frequency at which a defect "attempts" to

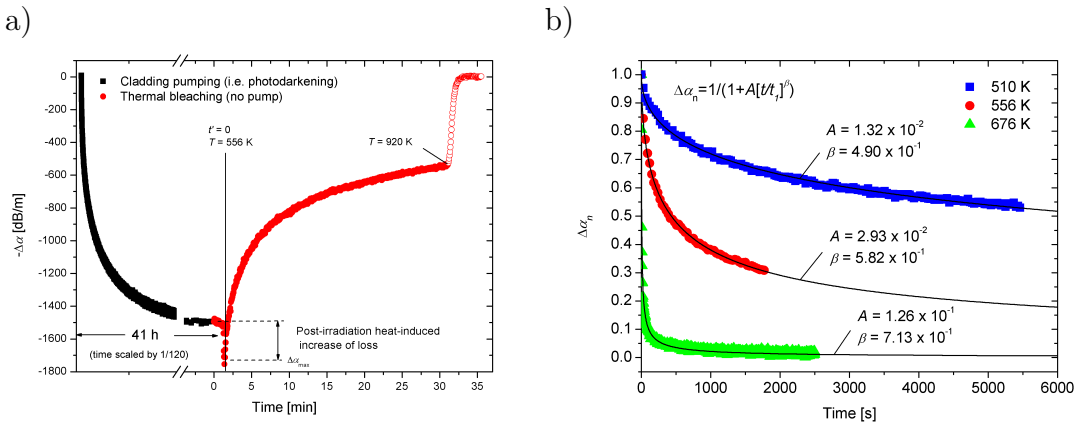


**Figure 5.4**: (a) A typical measurement cycle including photodarkening and isothermal bleaching of the induced losses and (b) change of normalized absorption coefficient $\Delta\alpha_n$ as a function of time at different temperatures.

escape from its potential energy well [91]. It is then convenient to reinterpret the experimental values of $\Delta\alpha_n$ in terms of $E_d$, as shown in Fig. 5.5. Using an attempt frequency of $\nu_0$=2.0 GHz, the various data sets (measured at different temperatures) can all be accurately parameterized by a single curve, referred to as the "demarcation energy curve". The dashed line represents a simple analytic dependence of the normalized absorption coefficient on $E_d$ [91]. The best fit parameters of this function indicate that the peak of the energy distribution $\Delta E$ is located at 1.32 eV. The inset graph presents the initial defect energy distribution, from which the full width half maximum (FWHM) of 0.31 eV can be obtained. For the other commercial LMA fiber, the demarcation energy curve yeilded $\nu_0$=2.0 GHz, $\Delta E$=1.50 eV, and FWHM=0.34 eV. Thermal bleaching of this sample was observed to initiate at ∼80 °C higher temperature, which is consistent with the higher observed activation energy. Reason for the difference in the activation energy between the two fibers is not well understood, but it is believed to be related to either compositional differences and/or differences in the thermal history of the fibers.

From Fig. 5.5 it can be understood, that each value of $\Delta\alpha_n$ is associated with a unique demarcation energy, with defects having energies less than $E_d$ are bleached,

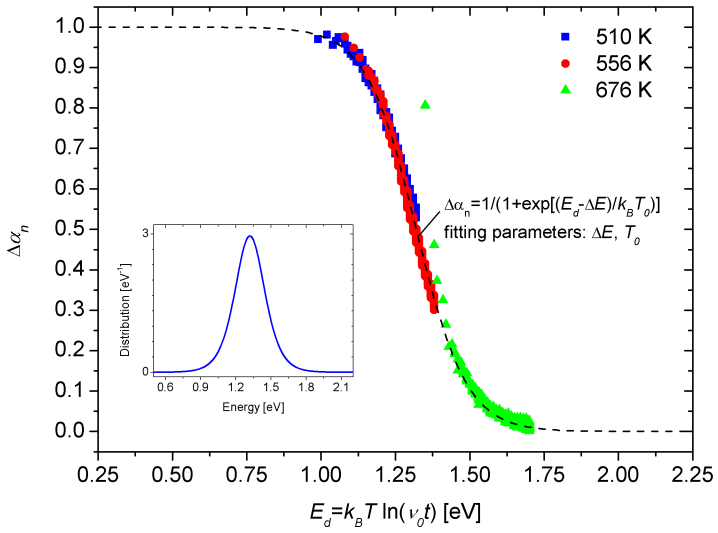


**Figure 5.5**: Demarcation energy curve (Publication V). The attempt frequency has been set to 2 GHz. Inset graph shows the initial defect energy distribution.

while defects having energy higher than $E_d$ remain unchanged. For example, a complete recovery of absorption (i.e. $\Delta\alpha_n \leq 0.01$) occurs at energies $\geq 1.9$ eV. Using Eq. 5.2, an appropriate combination of bleaching temperature and time can be derived to restore the sample back to its pre-photodarkened state (e.g. 600 °C for 47 s corresponds to energy of $\sim$1.9 eV). $\Delta\alpha_n$ begins to decrease at $\sim$1 eV, which suggests that thermal bleaching may also be expected to eventually occur even at moderate fiber temperatures (e.g. 50 °C), albeit very slowly. In parallel with (and independent of) the work presented in Publication V, Leich *et al.* studied the thermal energy distribution of photodarkening-induced defects using a non-isothermal method [89]. Thermal recovery curves using different temperature ramp rates were recorded, and the observed recovery behavior was modeled using a first order rate equation. Measurements taken at two different ramp rates allowed the extraction of the involved activation energy distribution. This distribution corresponded well with a Gaussian distribution with a mean value of 1.3 eV and a FWHM of 0.5 eV. These results are in excellent agreement with results presented in Publication V.

## 5.3 Fiber temperature measurement

In light of the various observed photodarkening-related thermal processes, characterization of the fiber temperature during pumping is of great interest. Knowledge of the fiber temperature can be used to estimate e.g. if the heat-induced darkening process is taking place during irradiation, what possible errors in the photodarkening rate measurement are caused by the spectral broadening of induced losses, and most interestingly, how temperature affects the equilibrium between the forward (i.e. photodarkening) and backward (thermal bleaching) processes. The sample fiber temperature was measured in-situ during cladding pumping using a high-resolution thermal camera (FLIR A320), which detects thermal emission in the long wavelength (8-12 $\mu$m) band and correlates it with the temperature of the emitting object. The camera with lenses was positioned some 3 cm over the sample and focused to give a sharp image of the sample. No cooling was applied to the sample. Figure 5.6(a) presents two measurements of induced loss at 600 nm and respective fiber temperatures using 5.7 W and 11 W of pump power at 915 nm. Several important observations can be made from this data set. The fiber temperature clearly correlates with progressing photodarkening, i.e., higher induced loss means higher fiber temperature. Fiber temperature exceeding 120 °C is measured upon the saturation of the loss at ∼1150 dB/m with 11 W of pump. Since the temperature with 5.7 W of pump power and the same loss level is significantly lower (80 °C), the mechanism for temperature increase appears to be related to both the pump power and to the level of induced loss. Figure 5.6(b) presents the fiber temperature increase versus a figure of merit for the lost pump power [$\Delta\alpha_{600nm} \times P_p$], for the two pump powers. The temperature increase is calculated versus fiber temperature at $\Delta\alpha_{600nm}$=0, extrapolated to be roughly 40 °C and 54 °C for 5.7 and 11 W of pump power, respectively. The two data sets overlap quite well, suggesting that the fiber temperature depends linearly on the pump power absorbed by the photodarkening-induced defects. A more detailed study involving the measured loss at the pump wavelength (i.e. $\Delta\alpha_{915nm}$) and a theoretical model for the fiber temperature distri-

bution [46] is under work. Initial modeling results indicate that the temperature gradient between the fiber core and the surface of the cladding is only a few degrees, and therefore the measured temperatures appear to represent good estimates of the actual core temperature.

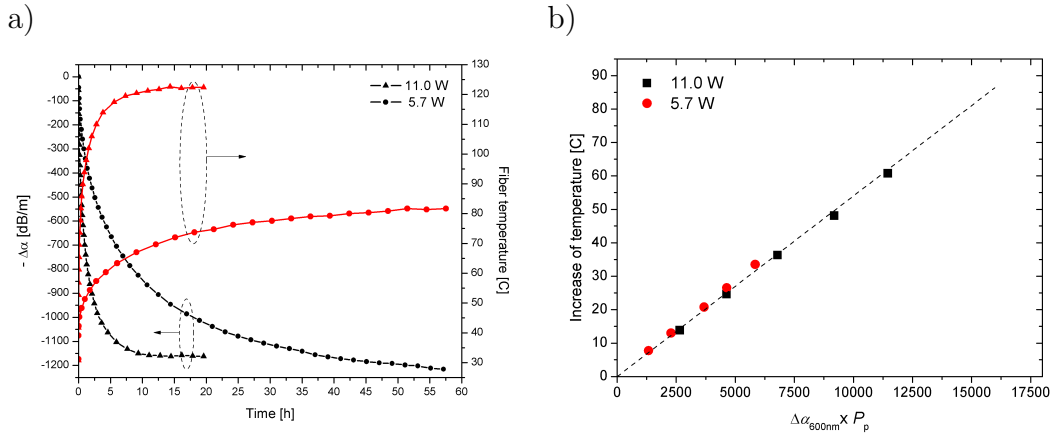


**Figure 5.6**: a) Photodarkening-induced change in the absorption coefficient and fiber temperature measured using 5.7 W and 11 W of pump power and (b) increase of fiber temperature plotted versus a figure of merit for lost pump power [$\Delta\alpha_{600nm}$ $\times$ $P_p$].

Another important observation from Fig. 5.6(a) is that the lower 5.7 W pump power (and therefore lower inversion) measurement exhibits more induced-loss. At about 57 hours of pumping, $\Delta\alpha_{600nm}$ is approximately 1220 dB/m, and is estimated to saturate to 1280 dB/m (using the stretched-exponential function), which is roughly 10 % more than with 11 W of pump power. While thermal bleaching can be expected to contribute to the difference in the observed loss levels due to the difference in fiber temperatures, contribution from other mechanisms, such as the temperature dependence of photodarkening precursors (i.e. concentration of possible defect sites), is also possible. Further evidence of the presence and effect of thermal bleaching is given by the comparison of the decay curve measured with 11 W of pump power with the decay curve shown in 5.4(a), measured with the same fiber and pump power, but with forced air cooling. Photodarkening in the cooled sample saturates

to 1450 dB/m in comparison to 1150 dB/m in the sample without air cooling. The same effect was observed by Leich *et al.* [73] who, instead of cooling, used external heating of the fiber. They observed faster rate of photodarkening with higher temperature, accompanied by lower degree of induced loss. It is finally pointed out that the observed dependence of saturated loss on inversion contradicts the results by Jetschke *et al.* [71], [85], who report on increasing loss with increasing level of inversion. This discrepancy is not well understood, but is possibly explained by the difference in cooling of the sample, i.e., a water bath was used by Jetschke to cool down the sample, whereas no cooling was applied here.

# 6 Mode-induced transverse photodarkening loss variations

The power-law dependence of photodarkening rate on inversion, discussed in section 4.1, has many implications on the performance of Yb-doped fiber lasers and amplifiers. One such possible manifestation is the transverse variation of the photodarkening rate, caused by the non-uniform inversion distribution in the core of an LMA fiber. A simulation study by Hotoleanu *et al.* [93] indicated that the rate of photodarkening is not uniform across a doped Yb-fiber core due to the inversion distribution defined by the pump and signal modes. In a practical fiber laser configuration, the core intensity distribution is largely determined by the lasing $LP_{01}$-mode. A commonly used bend loss discrimination of HOMs [7] causes the fundamental mode to distort and shift towards the outer edge of the core, as illustrated in Fig. 6.1(a). The consequent non-uniform inversion distribution is illustrated in Fig. 6.1(b). Regions of the core where the inversion-depleting $LP_{01}$-mode is low remain in high pump-induced inversion and hence experience higher rate of photodarkening than regions under the influence of the $LP_{01}$-mode. In Publication IV, photodarkening-induced changes were measured indirectly by comparing the near-field intensity distributions of the transmitted light of a pristine and a photodarkened fiber core. This measurement method is based on the principles of differential mode attenuation measurements developed for characterization of multimode optical fibers [94]. Measurements were done in the 450-650 nm wavelength range which coincides with the peak of the photodarkening loss. Results of these measurements are summarized in Figs. 6.2(a)-(b). In the case of core-pumping (without lasing), the intensity change distribution features a central higher loss region (within a radius of $\sim$6 $\mu$m), while in the case of a cladding pumped fiber laser, the loss is clearly more localized in the outer edge of the core. These distributions agree qualitatively with the calculated inversion profile shown in Fig. 6.1(b); in

a) b)

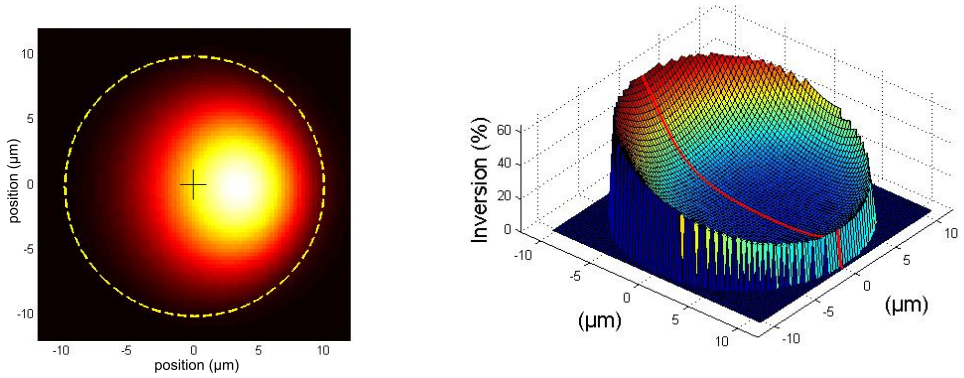


**Figure 6.1**: (a) Calculated $LP_{01}$-mode intensity distribution in a coiled 20-$\mu$m-core diameter LMA fiber and (b) calculated inversion distribution for a cladding pumped fiber laser based on the mode profile shown in (a).

cladding pumping, the highest inversion and therefore also the highest rate of photodarkening takes place at the edge of the core while the opposite is true for the core-pumped fiber. Further evidence for non-uniform photodarkening in an LMA fiber was provided by Koponen *et al.* [95], who observed a reduction in the slope power conversion efficiency (PCE) between a pristine fiber and a fiber that had been photodarkened in a fiber laser configuration, and then recoiled in the opposite direction. The decrease in the PCE was attributed to the increased overlap of the lasing $LP_{01}$-mode with the photodarkening distribution upon re-coiling of the fiber.

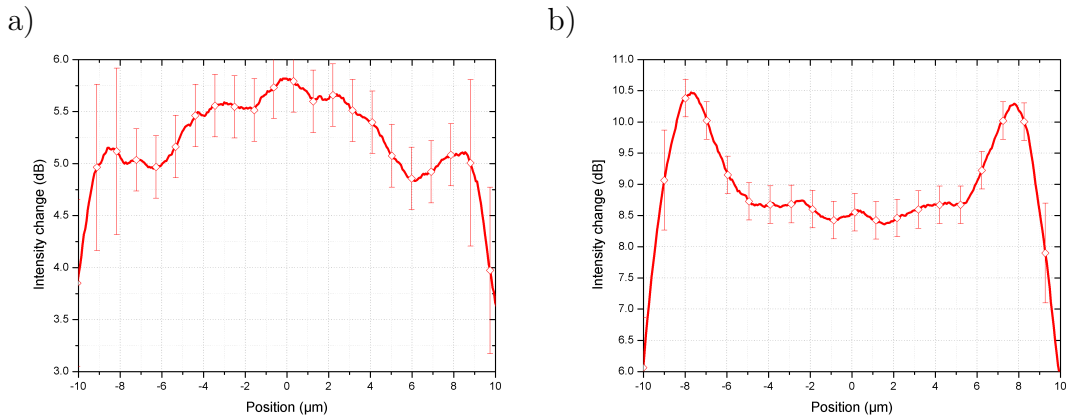


**Figure 6.2**: (a) Photodarkening-induced near-field intensity distribution change in a core-pumped LMA fiber and (b) in a cladding-pumped LMA fiber laser (Publication VI.

# 7 Discussion

Discrepancies between the ion-dependence derived in Publication III and results by Jetschke *et al.* [71],[85] are first addressed. The higher obtained ion-dependence of $[Yb^*]^7$ may partly be due to the insufficient measurement length, leading to a systematic error in the photodarkening parameters as was explained in [72]. A closer look at Fig. 4.2(b) indeed reveals a systematic deviation from the linear dependence (in a $\log(\tau^{-1})$-$\log(N_2)$ plot) expected for a simple $\tau^{-1} \propto [Yb^*]^n$ power-law dependence. The measured datapoints show a trend of an increasing deviation from linearity with increasing $\log(N_2)$. However, the same trend is also observed in ion-dependence plots by Jetschke *et al.* where, at least in [85], guidelines for the measurement length were reportedly obeyed. The results of this dissertation suggest that this trend is, in fact, related to the increase of fiber temperature, driven by pump power absorbed by the photodarkening-induced defects and enhanced by spectral loss broadening. The rate of thermal bleaching was observed in Publication V to depend exponentially on temperature. Thermal bleaching reduces the photodarkening-induced saturation loss level, therefore increasing the observed rate of photodarkening. Furthermore, temperature has been observed to directly increase the rate of photodarkening [73]. Regardless of which mechanism is dominant, significant temperature-related increase of the rate of photodarkening can be expected between measurements made at increasing pump powers (i.e. inversion levels). While the use of a water bath improves the heat extraction from the core of the fiber and therefore alleviates the thermal effects, it cannot completely eliminate the observed high temperature differences. Measurements in Publication III were done in a water bath, but the active fiber had a polymer coating with low thermal conductivity, effectively reducing the thermal conduction between the core of the fiber and the water bath. Therefore, a higher temperature-related artifact was observed in comparison to the work by Jetschke *et al.*, who had the active fiber uncoated in the water bath. Nevertheless, both measurements are believed to have been affected by uncontrolled temperature con-

ditions. It is finally noted, that Engholm *et al.* determined from the spectral shape of absorption in the UV-range that combined energy of 3-4 pump photons is needed to reach the charge transfer band energies [77]. Therefore, the results by Jetschke ($[Yb^*]^{4.6}$,[85]) are in fairly good agreement with these results.

The observed correlation between fiber temperature and pump power absorbed by the photodarkening-induced defects also raises questions regarding the validity of the reported photo-bleaching observations [68],[75], since these experiments were not reported to have been done under isothermal conditions. The wavelengths used, 355-nm and 534-nm, overlap with the broad peak of the induced loss, and the excitation source photons are therefore very efficiently absorbed by the loss inducing defects and dissipated as heat. Resulting increase of fiber temperature and subsequent thermal bleaching of induced losses can consitute a significant fraction of the observed recovery. And while Jetschke *et al.* observed the pump-induced photo-bleaching with the sample immersed in water during the course of the experiment [71], thermal assistance in the observed recovery cannot be fully ruled out. In light of the derived thermal activation energy (i.e. 1.3 eV), all such photo-bleaching measurements, as well as comparative photodarkening measurements, should be done under isothermal (and preferrably cooled to room temperature or colder) conditions to eliminate the uncertainty related to the presence of thermal bleaching. It is further noted that while the measured activation energy is close to the energy separation ($\sim$1.24 eV) of the Yb-ion ground $^2F_{7/2}$ and excited state manifolds $^2F_{5/2}$, this result does not necessarily imply that the transition is optically excited.

# 8 Summary and outlook

The aim of this dissertation was to characterize the photodarkening effect in ytterbium-doped silica fibers, and to develope quantifiable measurement methods to improve the understanding of the underlying photo-chemical mechanism. In Publication II, a photodarkening-induced loss spectrum was measured and a measurement method to benchmark the photodarkening behavior of different fibers was introduced. The induced loss spectrum was measured to exhibit near-exponential behavior toward the visible wavelength with a tail overlapping the 1.0 $\mu$m yb-ion operating wavelength. The room temperature loss ratio between a weak probe at 633 nm and 1.06 $\mu$m was found to be roughly 71.

A quantifiable measurement method for derivation of the photodarkening rate dependence on inversion was established in Publication III by the use of cladding pumping to produce a controllable, longitudinally and transversally uniform inversion distribution. Photodarkening rate curves measured at different inversion levels indicated inversion to be a key controlling variable in the forward photodarkening process. However, the measurement results were found to systematically deviate from a simple power-law dependence.

Three thermal processes were observed that affect the photodarkening kinetics and therefore complicate the interpretation of kinetic data. In Publication IV, the photodarkening-induced absorption spectrum was found to exhibit a heat-induced spectral broadening with the loss-change having a linear dependence on temperature proportional to $|\lambda\text{-}\lambda_0|$. For the studied fiber, $\lambda_0$ was found to be $\sim$612 nm. The observed spectral changes in the 550-850 nm spectral range were well explained by the temperature-dependent broadening of a single Gaussian-shaped absorbing species. Additionally, a photodarkened sample was measured to exhibit further heat-induced darkening prior to the initiation of thermal bleaching. Similarity of the spectral

shapes of induced losses indicated that this post-irradiation heat-induced darkening originates from the same type of a color center as is created through the NIR (e.g. 915 nm) pump excitation. Thermal bleaching was observed to initiate at 325 °C, with the full recovery of loss occuring at roughly 625 °C.

In Publication V, thermal activation energy distribution of photodarkening-induced defects was measured using the demarcation energy curve approach. This distribution was found to be governed by a single defect with the peak of the activation energy distribution located at 1.32 eV with a FWHM of ∼0.31 eV. Thermal energy of 1.9 eV was determined to completely restore a sample to its pre-photodarkened state. However, significant bleaching occurs at much lower energies (e.g. 1 eV), suggesting that thermal bleaching may also be expected to eventually occur even at moderate fiber temperatures (e.g. 50 °C), albeit slowly. The fiber temperature was measured with a thermal camera during the course of a photodarkening rate measurement. The uncooled sample fiber temperature was observed to increase with progressing photodarkening and reach 120 °C upon saturation of photodarkening. Temperature of the fiber was found to correlate with the pump power absorbed by the photodarkening-induced defects. The resulting increase of fiber temperature may be significant and therefore progessively activate the three observed thermal processes.

In Publication VI, a manifestation of the inversion dependence of photodarkening, i.e., transverse photodarkening-induced loss variation, was observed by comparing the near-field intensity distributions of pristine and photodarkened fibers. Observed higher photodarkening-induced loss at the edge of the core is qualitatively consistent with an inversion distribution in a cladding-pumped LMA Yb-fiber laser operating with the fundamental $LP_{01}$-mode.

In addition to the work related to photodarkening, a theoretical study on inversion, gain and amplified spontaneous emission behaviour in a cladding-pumped erbium-

doped fiber was conducted in Publication I. Counter-propagating amplified spontaneous emission in a double cladding L-band erbium-doped fiber amplifier was simulated to exhibit a strong dependence on the cladding area. Increasing the cladding area was found to result in a more uniform inversion distribution along the fiber length, therefore preventing short-wavelength gain and the ASE buildup and improving efficiency. These findings were also useful in the efforts to quantify the inversion dependence of photodarkening in Publication III.

This dissertation highlights the need to conduct kinetic photodarkening studies under isothermal conditions. Eliminating the temperature variations will allow determination of the true photodarkening rate dependence on inversion, which is crucial to the improved understanding of the underlying photo-chemical mechanism. It is then equally important to characterize the temperature-dependence of this process, and to clarify the respective roles of thermal bleaching and photo-bleaching in driving the equilibrium between the creation and bleaching of the loss-inducing defects. These efforts will lead to a broader understanding of the photodarkening mechanism which will facilitate the development of modeling capabilities and eventually the prediction of photodarkening behavior in a large variety of fiber laser configurations. This is important even in the light of the promising reports on themitigation of photodarkening by composition optimizations, as the design trade-offs involved may limit global fiber optimization options.

# References

[1] Y. Jeong, J. Sahu, D. Payne, and J. Nilsson, "Ytterbium-doped large-core fiber laser with 1.36 kW continuous-wave output power," Opt. Express **12**, 6088-6092 (2004).

[2] M.-Y. Cheng, K. Hou, A. Galvanauskas, D. Engin, R. Changkakoti, and P. Mamidipudi, "High average power generation of single-transverse mode MW-peak power pulses using 80-$\mu$m core Yb-doped LMA fibers," presented at the Conf. Lasers Electro-Opt., Long Beach, CA, 2006, Paper CThAA3.

[3] J. Limpert, F. Röser, T. Schreiber, and A. T*ü*nnermann, "High-Power Ultrafast Fiber Laser Systems," IEEE J. Sel. Top. Quantum Electron. **12**, 223-244 (2006).

[4] D. A. V. Kliner, F. Di Theodoro, J. P. Koplow, S. W. Moore, and A. V. Smith, "Efficient second, third, fourth and fifth harmonic generation of a Yb-doped fiber amplifier," Opt. Commun. **210**, 393-398 (2002).

[5] E. Snizer, H. Po, F. Hakimi, R. Tumminelli, and B. C. McCollum, "Double-clad, offset core Nd fiber laser," in Optical Fiber Sensors, vol. 2, OSA Technical Digest Series. Washighton, DC: Optical Society of America, 1988.

[6] M. Fermann, "Single-mode excitation of multimode fibers with ultrashort pulses," Opt. Lett. **23**, 52-54, 1998.

[7] P. Koplow, L. Goldberg, R. P. Moeller, and D. A. V. Kliner, "Singlemode operation of a coiled multimode fiber amplifier," Opt. Lett. **25**, 442-444, 2000.

[8] J. M. Sousa and O. G. Okhotnikov, "Multimode Er-doped fiber for single-transverse-mode amplification," Appl. Phys. Lett. **74**, 1528-1530 (1999).

[9] J. Koponen, M. Söderlund, S. Tammela, and H. Po, "Photodarkening in Ytterbium-Doped Silica Fibers", SPIE Europe Symposium Optics/Photonics in Security and Defence 2005, Bruges, Belgium, 5990-04 (2005).

[10] J. Nilsson and B. Jaskorzynska, "Modeling and optimization of low-repetition-rate high-energy pulse amplification in cw-pumped erbium-doped fiber amplifiers," Opt. Lett.**18** (1993).

[11] M. H. Muendel, "Optical fiber structure for efficient use of pump power," United States Patent 5,533,163, (1996).

[12] S. Bedö, W. L*ü*thy, and H. P. Weber, "The effective absorption coefficient in double-clad fibers", Opt. Commun. **99**, 331-335 (1993).

[13] D. J. DiGiovanni and A. J. Stentz, "Tapered fiber bundles for coupling light into and out of cladding-pumped fiber devices," United States Patent 5,864,644 (1999).

[14] T. Weber, W. L*ü*thy, and H. P. Weber, "Side-pumped fiber laser," Appl. Phys. B **63**, 131-134 (1996).

[15] J. P. Koplow, S. W. Moore, and D. A. V. Kliner, "A new method for side pumping of double-clad fiber sources," IEEE J. Quantum Electron. **39**, 529-540 (2003).

[16] V. P. Gapontsev and I. Samartsev, "Coupling arrangement between a multimode light source and an optical fiber through an intermediate optical fiber length," United States Patent 5,999,673 (1999).

[17] R. J. Mears, L. Reekie, I. M. Jauncey, and D. N. Payne, "Low-noise erbium-doped fiber amplifier operating at 1.54-$\mu$m," Electron. Lett. **23**, 1026-1028 (1987).

[18] E. Desurvire, J. R. Simpson, and P. C. Becker, "High-gain erbium-doped traveling-wave fiber amplifier," Opt. Lett. **12**, 888-890 (1987).

[19] E. Desurvire, Erbium-Doped Fiber Amplifiers. New York: Wiley, 1994.

[20] E. Snitzer and R. Woodcock, "$Yb^{3+}$-$Er^{3+}$ Glass Laser," Appl. Phys. Lett **6**, 45-46 (1965)

[21] D.Y. Shen , J. K. Sahu, W. A. Clarkson, "Highly efficient Er, Yb-doped fiber laser with 188 W free-running and >100 W tunable output power," Opt. Express. **13**, 4916-4921 (2005).

[22] R. Paschotta, J. Nilsson, A. C. Tropper, and D. C. Hanna, "Ytterbium-Doped Fiber Amplifiers," IEEE J.Quantum Electron. **33**, 1049-1056 (1997).

[23] P. F. Moulton, G. A. Rines, E. V. Slobodtchikov, K. F. Wall, G. Frith, B. Samson, and A. L. G. Carter, "Tm-Doped Fiber Lasers: Fundamentals and Power Scaling, " IEEE J. Sel. Top. Quantum Electron. **15**, 85-92 (2009).

[24] D. C. Hanna, R. M. Percival, I. R. Perry, R. G. Smart, P. J. Suni, J. E. Townsend, and A. C. Tropper, "Continuous-wave oscillation of a monomode ytterbium-doped fiber laser," Electron. Lett., vol. 24, pp. 1111-1113, 1988.

[25] S. Magne, Y. Ouerdane, M. Druetta, J. P. Goure, P. Ferdinand, and G. Monnom, "Cooperative luminescence in an ytterbium-doped silica fiber," Opt. Commun. **111**, 310-316 (1994).

[26] B. Schaudel, P. Goldner, M. Prassas, and F. Auzel, "Cooperative luminescence as a probe of clustering in $Yb^{3+}$-doped glasses," Journal of Alloys and Compounds 300-301, 443-449 (2000).

[27] J. Kirchhof, S. Unger, S. Jetschke, A. Schwuchow, M. Leich and V. Reichel,"Yb doped silica based lasers: correlation of photodarkening kinetics and related optical properties with glass composition," in proceedings of Fiber Lasers VI: Technology, Systems, and Applications, Denis V. Gapontsev, Dahv A. V. Kliner, Proc. SPIE 7195, 71950S41 (2009).

[28] B. Morasse, S. Chatigny, E. Gagnon, C. Hovington, J.-P. Martin, and J.-P. De Sandro, "Low photodarkening single cladding ytterbium fibre amplifier," in Fiber Lasers IV: Technology, Systems, and Applications, D. J. Harter, A. Tünnermann, J. Broeng, and C. Headley, Proc. SPIE 6453, 64530H-1-9 (2007).

[29] J.D. Dawson, M. J. Messerly, R. J. Beach, M. Y. Shverdin, E. A. Stappaerts, A. K. Sridharan, P. H. Pax, J. E. Heebner, C. W. Siders and C. P. J. Barty, "Analysis of the scalability of diffraction-limited fiber lasers and amplifiers to high average power," Opt. Express **16**, 13240-13266 (2008).

[30] R. Paschotta, J. Nilsson, P.R. Barber, J.E. Caplen, A.C. Tropper, D.C. Hanna, "Lifetime quenching in Yb doped fibres," Opt. Commun. **136**, 375-378 (1997).

[31] P. C. Becker, N. A. Olsson, and J. R. Simpson, "Erbium-doped Fiber Amplifiers: Fundamentals and Technology," Academic Press (1999).

[32] D. Marcuse, "Field deformation and loss caused by curvature of optical fibers," J. Opt. Soc. Am. **66**, 216 (1976).

[33] V. Filippov, Y. Chamorovskii, J. Kerttula, A. Kholodkov, and O. G. Okhotnikov, "600 W power scalable transverse mode tapered double-clad fiber laser," Opt. Express **17**, 1203-1214 (2009)

[34] Chi-Hung Liu, Guoqing Chang, Natasha Litchinister, Doug Guertin, Nick Jacobson, Kanishka Tankala, and Almantas Galvanauskas, "Chirally Coupled Core Fibers at 1550-nm and 1064-nm for Effectively Single-Mode Core Size Scaling," CLEO/QELS (OSA 2007), paper CTuBB3.

[35] B. J. Ainslie, "A Review of the Fabrication and Properties of Erbium-doped Fibers for Optical Amplifiers," J. Lightwave Technol. **9**, 220-227 (1991).

[36] P. C. Schultz, "Fabrication of Optical Waveguides by the Outside Vapor Deposition Process," Proc. of the IEEE **68**, 1187-1190 (1980).

[37] S. Tammela, P. Kiiveri, S. Särkilahti, M. Hotoleanu, H. Valkonen, M. Rajala, J. Kurki, adn K. Janka, "Direct Nanoparticle Deposition Process for manufacturing very shor high gain Er-doped silica glaa fibers," Proc. European Conference on Optical Communications ECOC'02 (IEEE 2002) 4, 1-2 (2002).

[38] R. P. Tumminelli, B. C. McCollum, and E. Snitzer, "Fabrication of High-Concentration Rare-Earth Doped Optical Fibers Using Chelates", J. Lightwave Technol. **8**, 1680-1683 (1990).

[39] J. Kirchhof, S. Unger, A. Schwuchow, S. Grimm, and V. Reichel, "Materials for high-power fiber lasers," J. Non-Cryst. Solids **352**, 2399-2403 (2006).

[40] S. Tammela, M. Söderlund, J. Koponen, V. Philippov, and P. Stenius, "The potential of Direct Nanoparticle Deposition for the Next Generation of Optical Fibers," in Optical Components and Materials III, M. J. Digonnet, S. Jiang, Proc. SPIE 6116, 61160G (2006).

[41] S. Tammela, M. Hotoleanu, P. Kiiveri, H. Valkonen, S. Särkilahti, K. Janka, "Very short Er-doped silica glass fiber for L-band amplifiers," Technical Digest of the Optical Fiber Communication Conference OFC, 1, 376-377, 2003.

[42] J. Limpert, F. Röser, S. Klingebiel, T. Schreiber, C. Wirth, T. Peschel, R. Eberhardt, and A. T*ü*nnermann, "The Rising Power of Fiber Lasers and Amplifiers," IEEE J. Sel. Top. Quantum Electron. **113**, 537-545 (2007).

[43] M. Dubinskii, J. Zhang, I. Kudryashov, "Single-Frequency, Yb-free, Resonantly Cladding-pumped LMA Er Fiber Amplifier for Power Scaling", Appl. Phys. Lett. **93**, 031111 (2008).

[44] M. Dubinskii, J. Zhang, and V. Ter-Mikirtychev, "Power scaling of resonantly cladding-pumped Er-doped narrow bandfiber lasers and amplifiers", in Conference on Lasers and Electro-Optics-European Quantum Electronics Conference CLEO/EUROPE-EQEC (OSA 2009), CJ2.2.

[45] L. Zenteno, "High-power double-clad fiber lasers," J. Lightwave Technol. **11**, 1435-1446 (1993).

[46] C. D. Brown and H. J. Hoffman, "Thermal, Stress, and Thermo-Optic Effects in High Average Power Double-Clad Silica Fiber Lasers," IEEE J. Sel. Top. Quantum Electron., **37**, 207-217 (2001).

[47] G. P. Agrawal, Nonlinear Fiber Optics. San Diego, CA: Academic, 1995.

[48] A. V. Smith and B. T. Do, "Deterministic Nanosecond Laser-Induced Breakdown Thresholds in Pure and $Yb^{3+}$ Doped Fused Silica", in Fiber Lasers IV: Technology, Systems, and Applications, edited by D. J. Harter, A. Tünnermann, J. Broeng, and C. Headley, Proc. SPIE 6453, 645317 (2007).

[49] V. Gapontsev, D. Gapontsev, N. Platonov, O. Shkurkhin, V. Fomin, A. Mashkin, M. Abramov, and S. Ferin, "2 kW CW ytterbium fiber laser with record diffraction limited brightness," in Proceedings of the Conference on Lasers and Electro-Optics Europe (OSA 2005).

[50] C. R. Giles and E. Desurvire, "Modeling erbium-doped fiber amplifiers," J. Lightwave Technol., **9**, 271-283 (1991).

[51] B. Pedersen, A. Bjarklev, J. H. Povlsen, K. Dybdal, and C. C. Larsen, "The design of erbium-doped fiber amplifiers," J. Lightwave Technol. **9**, 1105-1112,(1991).

[52] A. A. Saleh, R. M. Jopson, J. D. Evankow, and J. Aspell, "Modeling of Gain in Erbium-Doped Fiber Amplifiers," IEEE Photon. Technol. Lett. **2**, 714-717 (1990).

[53] A. A. Hardy and R. Oron, "Amplified spontaneous emission and Rayleigh backscattering in strongly pumped fiber amplifiers," J. Lightwave Technol. **16**, 1865-1873 (1998).

[54] P. Bousselet, M. Bettiati, L. Gasca, M. Goix, F. Boubal, C. Sinet, F. Leplingard, and D. Bayart, "+26-dBm output power from an engineered cladding-pumped Yb-free EDFA for L-band WDM applications," in OFC/IOOC '99. Tech. Dig., 1999, Paper WG5-1.

[55] F. Di Pasquale, G. Grasso, F. Meli, G. Sacchi, and S. Turolla, "23-dBm output power Er/Yb co-doped fiber amplifier for WDM in the 1575-1605 nm wavelength region," in OFC/IOOC '99. Tech. Dig., 1999, Post-deadline Paper WA2-1.

[56] J. F. Massicott, J. R. Armitage, R. Wyatt, B. J. Ainslie, and S. P. Craig-Ryan, "High gain, broadband, 1.6-$\mu$m $Er^{3+}$-doped silica fiber amplifier," Electron. Lett. **26**, 1645-1646 (1990).

[57] H. Ono, M. Yamada, and Y. Ohishi, "Gain-flattened Er-doped fiber amplifier for a WDM signal in the 1.571.60-$\mu$m wavelength region," IEEE Photon. Technol. Lett. **9**, 596-598 (1997).

[58] F. A. Flood and C. C. Wang, "980-nm pump-band wavelengths for long-wavelength-band erbium-doped fiber amplifiers," IEEE Photon. Technol. Lett. **11**, 1232-1234 (1999).

[59] J. Koponen, M. Laurila, and M. Hotoleanu, "Inversion behavior in core- and cladding-pumped Yb-doped fiber photodarkening measurements," Appl. Opt. **47**, 4522-4528 (2008).

[60] L. B. Glebov, "Linear and Nonlinear Photoionization of Silicate Glasses," Glass Sci. Technol. **75**, C2 (2002).

[61] M. M. Broer, D. M. Krol, and D. J. DiGiovanni, "Highly nonlinear near-resonant photodarkening in a thulium-doped aluminosilicate glass fiber," Opt. Lett. **18**, 799-801 (1993).

[62] E. G. Behrens and R. C. Powell, "Characteristics of laser induced gratings in $Pr^{3+}$- and $Eu^{3+}$-doped silicate glasses," J. Opt. Soc. Am. B **7**, 1437-1444 (1990).

[63] M. M. Broer, R. L. Cone, and J. R. Sompson, "Ultraviolet-induced distributed-feedback gratings in $Ce^{3}$-doped silica optical fibers," Opt. Lett. **16**, 1391-1393 (1991).

[64] G. R. Atkins, and A. L. G. Carter, "Photodarkening in $Tb^{3+}$-doped phosphosilicate and germanosilicate optical fibers," Opt. Lett. **19**, 874-876 (1994).

[65] J. J. Koponen, M. J. Söderlund, S. K. Tammela, and H. Po, "Photodarkening in ytterbium-doped silica fibers," Proc. SPIE 5990, 599008 (2005).

[66] K. E. Mattson, S. N. Knudsen, B. Cadier, and T. Robin, "Photo darkening in ytterbium co-doped silica material," Fiber Lasers V: Technology, Systems, and Applications, J. Broeng, C. Headley, D. V. Gapontsev, and D. Kliner, Proc. SPIE 6873, 6873-48 (2008).

[67] T. Kitabayashi, M. Ikeda, M. Nakai, T. Sakai, K.Himeno, and K. Ohashi, "Population inversion factor dependence of photodarkening of Yb-doped fibers and its suppression by highly aluminum doping," in OFC/NFOE Conference (OSA 2006), paper OThC5.

[68] I. Manek-Hönninger, J. Boullet, T. Cardinal, F. Guillen, M. Podgorski, R. Bello Doua, and F. Salin, "Photodarkening and photobleaching of an ytterbium-doped silica double-clad LMA fiber," Opt. Express **15**, 1606-1611 (2007).

[69] J. Koponen, M. Söderlund, H. J. Hoffman, D. Kliner, and J. Koplow, "Photodarkening measurements in large-mode-area fibers," in Fiber Lasers IV: Technology, Systems, and Applications, D. J. Harter, A. Tünnermann, J. Broeng, and C. Headley, Proc. SPIE 6453, 64531E-1-11 (2007).

[70] A. V. Shubin, M. V. Yashkov, M. A. Melkumov, S. A. Smirnow, I. A. Bufetov, and E. M. Dianov, "Photodarkening of aluminosilicate and phosphosilicate Yb-doped fibers," in Conf. Digest of CLEO Europe-EQEC 2007, CJ3-1-THU.

[71] S. Jetschke, S. Unger, U. Röpke, J. Kirchhof, "Photodarkening in Yb doped fibers: experimental evidence of equilibrium states depending on the pump power," Opt. Express **15**, 14838-14843 (2007).

[72] S. Jetschke, U. Röpke, "Power-law dependence of the photodarkening rate constant on the inversion in Yb doped fibers," Opt. Lett. **34**, 109-111 (2009).

[73] M. Leich, S. Jetschke, S. Unger, and V. Reichel, "Acceleration of photodarkening measurements in Yb-doped fibers by enhanced temperaturs," in Conference on Lasers and Electro-Optics-European Quantum Electronics Conference CLEO/EUROPE-EQEC (OSA 2009), CE.P.29.

[74] J. Jasapara, M. Andrejco, D. DiGiovanni, and R. Windeler, "Effect of heat and H2 gas on the photodarkening of $Yb^{3+}$ fibers," in Conference on Lasers and Electro-Optics/Quantum Electronics and Laser Science Conference and Photonic Applications Systems Technologies 2006, Technical Digest (OSA 2006), paper CTuQ5.

[75] A.D. Guzman Chàvez, A.V. Kir'yanov, Yu.O. Barmenkov, and N.N. Il'ichev, "Reversible photo-darkening and resonant photobleaching of Ytterbium-doped silica fiber at in-core 977-nm and 543-nm irradiation", Laser Phys. Lett. **4**, 734-739 (2007).

[76] M. Engholm, L. Norin, and D. Åberg, "Strong UV absorption and visible luminescence in ytterbium-doped aluminosilicate glass under UV excitation," Opt. Lett. **32**, 3352-3354 (2007).

[77] M. Engholm and L. Norin, "Preventing photodarkening in ytterbium-doped high power fiber lasers; correlation to the UV-transparency of the core glass," Opt. Express **16**, 1260-1268 (2008).

[78] S. Yoo, C. Basu, A. J. Boyland, C. Sones, J. Nilsson, J. K. Sahu, and D. Payne, "Photodarkening in Yb-doped aluminosilicate fibers induced by 488nm irradiation," Opt. Lett. **32**, 1626-1628 (2007).

[79] M. Engholm and L. Norin, "Comment on "Photodarkening in Yb-doped aluminosilicate fibers induced by 488-nm irradiation"," Opt. Lett. **33**, 1216-1216 (2008).

[80] S. Yoo, C. Basu, A. J. Boyland, C. Sones, J. Nilsson, J. K. Sahu, and D. Payne, "Reply to comment on "Photodarkening in Yb-doped aluminosilicate fibers induced by 488-nm irradiation"," Opt. Lett. **33**, 1217-1218 (2008).

[81] T. Arai, K. Ichii, S. Tanigawa and M. Fujimaki, "Defect Analysis of Photodarkened and Gamma-Ray Irradiated Ytterbium-Doped Silica Glasses, " in OFC/NFOEC Conference (OSA 2009), paper OWT2.

[82] S. Jetschke, S. Unger, A. Schwuchow, M. Leich, and J. Kirchhof, "Efficient Yb laser fibers with low photodarkening by optimization of the core composition," Opt. Express **16**, 15540-15545 (2008).

[83] M. Engholm, P. Jelger, F. Laurell, and L. Norin, "Improved photodarkening resistivity in ytterbium-doped fiber lasers by cerium codoping," Opt. Lett. **34**, 1285-1287 (2009).

[84] P. Laperle, L. Desbiens, K. Le Foulgoc, M. Drolet, P. Deladurantaye, A. Proulx, and Y. Taillon, "Modeling the photodegradation of large mode area Yb-doped fiber power amplifiers" Fiber Lasers VI: Technology, Systems, and Applications, D. V. Gapontsev, D. A. V. Kliner, J. W. Dawson, and K. Tankala, Proc. SPIE 7195, 71952C-1 (2009).

[85] S. Jetchke, U. Röpke, S. Unger, and J. Kirchhof, "Characterization of photodarkening processes in Yb doped fibers," Fiber Lasers VI: Technology, Systems, and Applications, D. V. Gapontsev, D. A. V. Kliner, J. W. Dawson, and K. Tankala, Proc. SPIE 7195, 71952B-1 (2009).

[86] J. J. Montiel i Ponsoda, M. J. Söderlund, J. Koplow, J. Koponen, A. Iho, and S. Honkanen, "Combined photodarkening and thermal bleaching measurement of an ytterbium-doped fiber," in proceedings of Fiber Lasers VI: Technology, Systems, and Applications, Denis V. Gapontsev, Dahv A. V. Kliner, Proc. SPIE 7195, 71952D-1-7 (2009).

[87] J. K. Sahu, S. Yoo, A. J. Boyland, M. P. Kalita, C. Basu, A. Webb, C. L. Sones, J. Nilsson, and D. N. Payne, "488 nm irradiation induced photodarkening study of Yb-doped aluminosilicate and phosphosilicate fibers," CLEO USA (2008).

[88] C. Basu, S. Yoo, A. J. Boyland, A.S. Webb, C. L. Sones , and J. K. Sahu, "Influence of temperature on the post-irradiation temporal loss evolution in Yb-doped aluminosilicate fibers, photodarkened by 488 nm CW irradiation," in Conference on Lasers and Electro-Optics-European Quantum Electronics Conference CLEO/EUROPE-EQEC (OSA 2009), CJ1.2.

[89] M. Leich, U. Röpke, S. Jetschke, S. Unger, V. Reichel, and J. Kirchhof, "Non-isothermal bleaching of photodarkened Yb-doped fibers, " Opt. Express **17**, 12588-12593 (2009).

[90] M. J. Söderlund, J. J. Montiel i Ponsoda, and S. Honkanen, "Measurement of thermal binding energy of photodarkening-induced color centers in ytterbium-doped silica fibers," in Conference on Lasers and Electro-Optics-European Quantum Electronics Conference CLEO/EUROPE-EQEC (OSA 2009), CE3.3.

[91] T. Erdogan, V. Mizrahi, P. J. Lemaire, and D. Monroe, "Decay of ultraviolet-induced fiber Bragg gratings," J. Appl. Phys. **76**, 73-80 (1994).

[92] S. Kannan, M. LuValle, R. Ahrens and P. Lemaire, "Analysis of recovery in radiation induced loss in rare earth doped fibers through master curve/demarcation energy diagrams," in Optical Fiber Communication Con-

ference, Vol. 3 of OSA Technical Digest Series (Optical Society of America, 1999), paper ThG5-1.

[93] M. Hotoleanu, J. Koponen, T. Kokki, "Spatial Distribution of Photodarkening in Large Mode Area Ytterbium Doped Fibers," in Advanced Solid-State Photonics Conference 2008, Technical digest (Optical Society of America, 2008), paper WE23.

[94] R. Olshansky and S. M. Oaks, "Differential mode attenuation measurements in graded-index fibers," Appl. Opt. **17**, 1830-1835 (1978).

[95] J. Koponen, M. Laurila and M. Hotoleanu, "Demonstration of spatial distribution of photodarkening in Yb-doped large-mode-area fibre laser, " Elect. Lett. **44**, 16 (2008).

ISBN 978-952-248-247-1
ISBN 978-952-248-248-8 (PDF)
ISSN 1795-2239
ISSN 1795-4584 (PDF)